Zhang *et al. Energy Mater.* **2025**, *5*, 500014
DOI: 10.20517/energymater.2024.42

Energy Materials

Review

Open Access

Check for updates

Modulating single-atom M-N-C electrocatalysts for the oxygen reduction: the insights beyond the first coordination shell

Dingliang Zhang[1], Xianyang Zhang[1], Xingchuan Li[1], Chang Feng[1], Yingying Chu[2], Cheng Chen[1,*], Zongkui Kou[1,*]

[1]State Key Laboratory of Advanced Technology for Materials Synthesis and Processing, Wuhan University of Technology, Wuhan 430070, Hubei, China.
[2]School of Chemistry, Chemical Engineering and Life Sciences, Wuhan University of Technology, Wuhan 430070, Hubei, China.

***Correspondence to:** Prof. Zongkui Kou, State Key Laboratory of Advanced Technology for Materials Synthesis and Processing, Wuhan University of Technology, Luoshi Road 122, Wuhan 430070, Hubei, China. E-mail: zongkuikou@whut.edu.cn; Dr. Cheng Chen, State Key Laboratory of Advanced Technology for Materials Synthesis and Processing, Wuhan University of Technology, Luoshi Road 122, Wuhan 430070, Hubei, China. E-mail: chengchen@whut.edu.cn

How to cite this article: Zhang, D.; Zhang, X.; Li, X.; Feng, C.; Chu, Y.; Chen, C.; Kou, Z. Modulating single-atom M-N-C electrocatalysts for the oxygen reduction: the insights beyond the first coordination shell. *Energy Mater.* **2025**, *5*, 500014. https://dx.doi.org/10.20517/energymater.2024.42

Received: 6 May 2024 **First Decision:** 24 Jun 2024 **Revised:** 14 Jul 2024 **Accepted:** 17 Jul 2024 **Published:** 9 Jan 2025

Academic Editor: Wei Tang **Copy Editor:** Fangling Lan **Production Editor:** Fangling Lan

Abstract

The oxygen reduction reaction (ORR) is a pivotal process in electrochemical energy systems such as fuel cells and metal-air batteries. Recent advancements have highlighted the single-atom metal-nitrogen-carbon (M-N-C) catalysts for their exceptional ORR electrocatalytic performance. However, further exploration is needed for the optimization methods of single atomic active sites. Significantly, the modulation of coordination environment emerges as a pivotal technique for the enhancement of M-N-C catalysts, while extending this modulation beyond the first coordination shell has ignited substantial investigation. This review delves into the frontier of M-N-C optimization by transcending the first coordination shell, presenting a comprehensive analysis of innovative strategies that modulate the electronic structure and reactivity of MN_4 sites. The primary focus lies in three regulation approaches: regulating atomic entities, introducing metallic species and tailoring non-metallic modulators. These strategies are scrutinized for their ability to fine-tune the ORR activity and stability at the atomic level. By providing a clearer trajectory for future research, this review should be able to inspire novel designs of high-performance M-N-C ORR catalysts.

Keywords: Oxygen reduction reaction, M-N-C electrocatalysts, coordination shell

INTRODUCTION

The global energy landscape is undergoing a transformative shift towards sustainable sources, necessitating advancements in energy conversion technologies. The electrochemical reduction of oxygen (ORR) plays a crucial role in the advancement of future renewable energy storage and conversion technologies, including fuel cells and metal-air batteries[1-3]. However, the inherent challenge with the ORR process lies in its sluggish kinetics, which originates from the intricate multi-step electron transfer process and inefficient mass transfer process. Currently, ORR is primarily categorized into two main processes based on electron transfer numbers: the $2e^-$ process and the $4e^-$ process[4]. When oxygen accepts two electrons and is incompletely reduced to hydrogen peroxide, it not only results in a decrease in energy conversion efficiency but also causes deactivation of catalysts and deterioration of devices through the attack of free radicals. In other words, we ought to develop ORR electrocatalysts with superior $4e^-$ selectivity in order to achieve better performance in energy conversion systems.

Single-atom metal-nitrogen-carbon (M-N-C) catalysts, with atomically precisely designed active sites and conductive carbon frameworks, are promising candidate materials for usage in renewable energy devices[5,6]. The unique microstructure of M-N-C catalysts, facilitated by the coordination of transition metals with nitrogen in a carbon matrix, is central to their ORR activity. Further research revealed that the MN_4 structure contributes most significantly to the reactivity of the $4e^-$ process[7-9]. Nevertheless, this extensively studied scaffold lacks the optimal adsorption behavior for oxygen and oxygen-containing intermediates and is susceptible to deactivation during the operation of electrochemical devices. Therefore, optimizing the activity and stability of M-N-C catalysts via structural design and modification is of crucial significance in advancing the ORR performance.

The core of regulating the catalytic performance of M-N-C lies in the modification of the electronic structure, which is closely related to the metal center and its coordination environment[10]. In transition metal elements, Fe and Co exhibit superior intrinsic ORR activity over the other non-noble metals[11]. However, isolated MN_4 sites struggle to match the performance of Pt/C, and it is difficult to achieve a balance between activity and stability. Consequently, numerous studies endeavored to modify the electronic structure by altering the coordination environment, aiming to optimize the interaction between the metal centers and oxygen-containing intermediates, and furthermore, address the trade-off issue. With intensive research focusing on the modification of the first coordination shell, such as the substitution of N in MN_4 to other heteroatoms[12-14], the addition of axially coordinated atoms[15,16], *etc*., we highlight the significance of modification in the outer coordination shell which possesses a more delicate regulation effect.

Expanding the scope of modification beyond the first coordination sphere opens up a new dimension of possibilities. By adjusting coordination environment in the second or higher shells, it is plausible to exert a more subtle yet profound influence on the MN_4 sites. In this review, we categorize the approaches for regulating MN_4 in the high coordination layer as follows [Figure 1]: (1) Adjusting atomic entities, encompassing the impact of atoms in the second shell or dispersed in the carbon framework, as well as the intrinsic order on the activity-stability trade-off of MN_4 sites; (2) Incorporating metallic species such as nanoclusters or nanoparticles to effectively modulate the electronic structure of MN_4 and function as radical scavengers; and (3) Introducing non-metallic modulators, including atomic defects and functional groups, to enhance ORR activity at MN_4 sites. We focus on exploring these outer coordination sphere modifications, aiming to unveil the full potential of M-N-C catalysts for ORR applications.

REGULATING ATOMIC ENTITIES BEYOND THE FIRST COORDINATION SHELL

In the local microstructure of heterogenous single-atom catalytic sites, it is crucial to define the

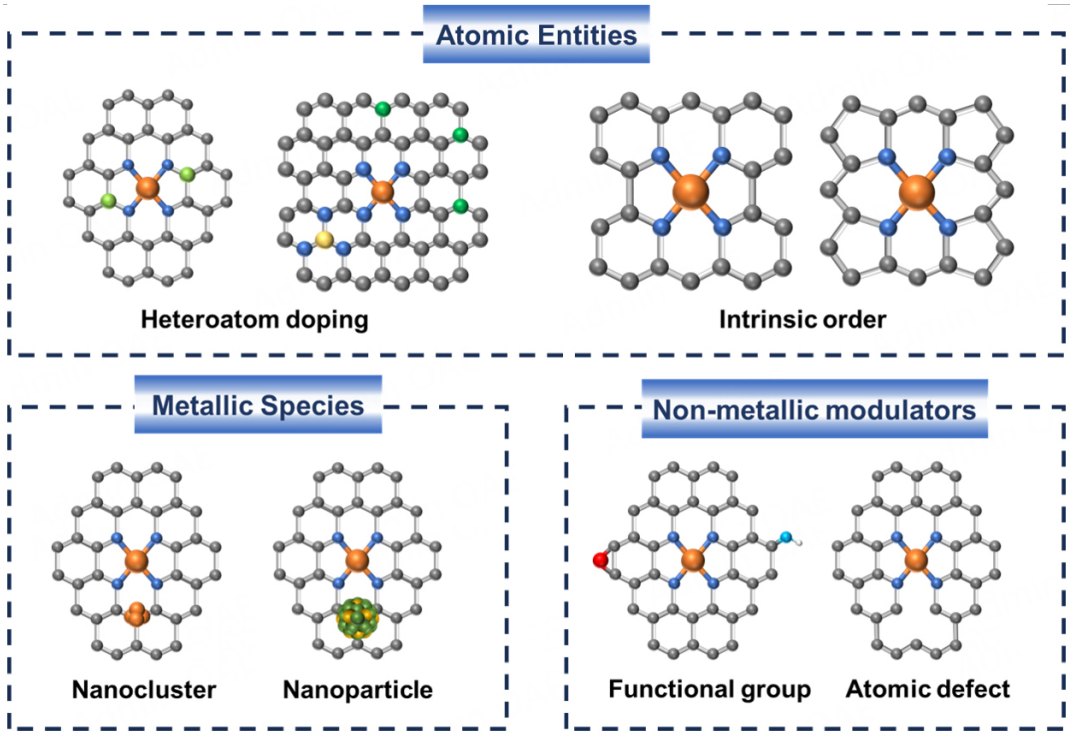

Figure 1. Schematic depiction of modulation approaches beyond the first coordination shell.

configuration of coordination environment. For the outer shells of MN_4, only the introduced atoms in the second shell can be accurately detected within the limits of current characterization methods[17]. However, atoms in the whole microenvironment surrounding MN_4 exhibit potential to regulate active centers and thus it is momentous to explore the modulation method for meticulously tailoring the reactivity. In this section, we first discuss the introduced atomic entities altering original carbon atoms in the outer coordination shell, including second and higher shells' atoms. On the other hand, the intrinsic order of local construction is deliberated, highlighting the inherent activity and stability exchange of catalytic sites.

Introducing the doped atoms

Designing atoms in the second shell

Atoms in the second coordination shell significantly affect the active center, and the introduction of other atomic entities disrupts the original electronic and geometric symmetry, thereby altering and optimizing the adsorption of ORR intermediates. Substituting light heteroatoms for the carbon atoms surrounding MN_4 is a straightforward and efficient approach to modulate the electronic structure of the monometal center[18-20]. For instance, Qin *et al.* introduced S anions in the second coordination shell [Figure 2A], effectively manipulating the electronic structure of the central metal Ru[21]. X-ray absorption near-edge structure (XANES) fitting based on optimized density functional theory (DFT) models indicated unambiguously that S atoms were confirmed to coordinate with N atoms [Figure 2B and C]. The asymmetrical expansion from RuN_4 to RuN_4S weakened the adsorption of ORR intermediates at Ru sites, enhancing ORR performance with a half-wave potential ($E_{1/2}$) of 0.861 V in alkaline media, surpassing that of Pt/C (0.853 V). Many studies have also demonstrated the positive impact of doping heteroatoms such as P[22], S[23] and O[24] into the second coordination layer of the central metal. Chen *et al.* elucidated the effect of S doping in the second coordination layer on the spin state of iron in FeN_4 sites[23]. ^{57}Fe Mössbauer spectroscopy demonstrated that neighboring S prominently increased the content of low-spin Fe^{3+} sites (D1) [Figure 2D], which possesses

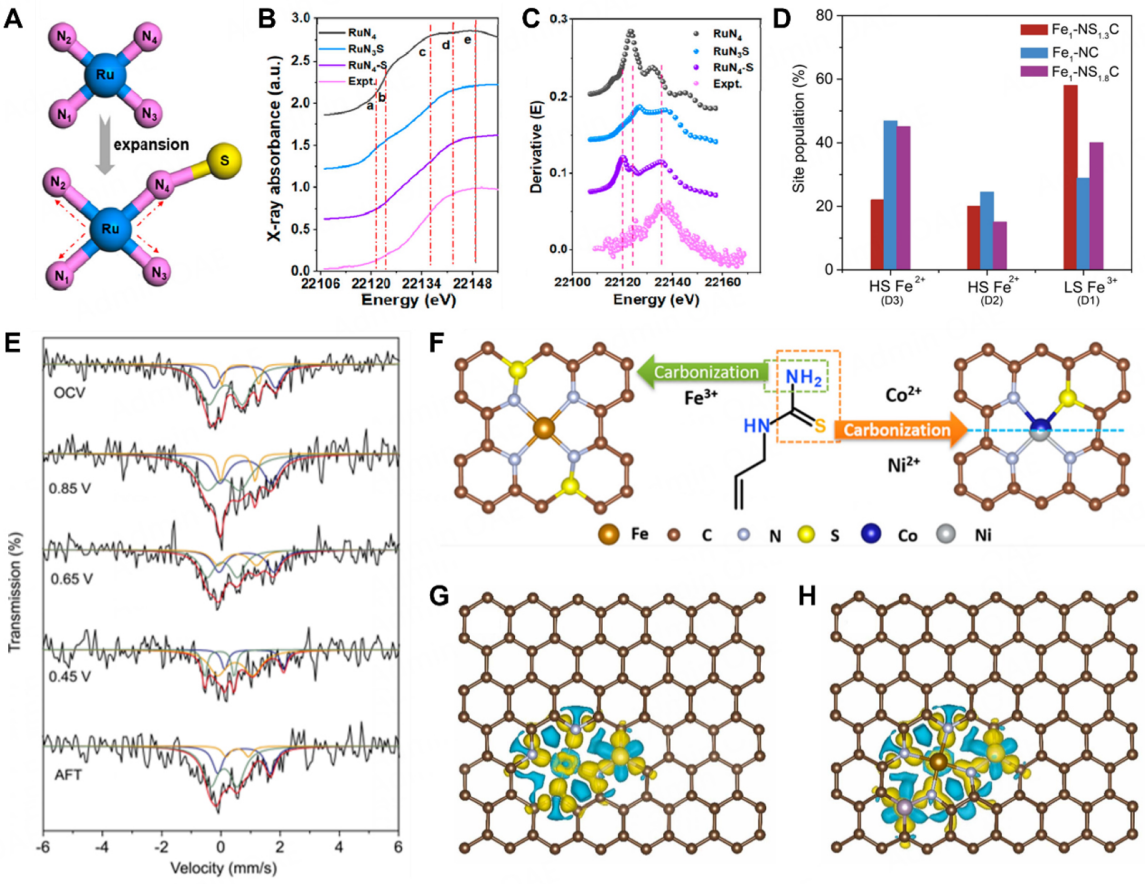

Figure 2. (A) Schematic atomic model of asymmetrical expansion from RuN_4 to RuN_4S. Reproduced with permission[21]. Copyright 2022, American Chemical Society. Comparison of Ru K-edge XANES spectrum (B) and the E-space derivation (C) between the experimental and theoretical fitting. Reproduced with permission[21]. Copyright 2022, American Chemical Society. (D) Content of Fe moieties with varied spin polarization deriving from ^{57}Fe Mössbauer spectroscopy. Reproduced with permission[23]. Copyright 2021, John Wiley and Sons. (E) The correlation between ORR overpotential (η_{ORR}) and OH* adsorption free energy (ΔG_{OH^*}) on Fe moieties with distinct local configurations. Reproduced with permission[23]. Copyright 2021, John Wiley and Sons. (F) Schematic illustration of the formation of Fe single-atom sites with different numbers and locations of S doping. Reproduced with permission[26]. Copyright 2019, American Chemical Society. Charge density difference of $Fe_1N_4P_1$ (G) and $Fe_1N_4P_2$ (H). The brown, blue, and golden spheres represent carbon, nitrogen, and iron atoms, respectively. Reproduced with permission[28]. Copyright 2023, Elsevier.

favorable adsorption strength for ORR intermediates owing to lowered e_g filling[25]. This was also confirmed in the operando Mössbauer spectrum [Figure 2E]. Upon applying different voltages, D1 sites underwent the transition in the spin polarization, indicating its activation of O_2 molecules as active sites. Further DFT calculations certified that the appropriate amount of S doping effectively facilitated the desorption process of OH* species, leading to an enhancement for the ORR catalytic activity. Zhang *et al.* distinguished structural differences between Co/Ni-centered and Fe-centered single atomic active sites[26]. The lower coordination tendency of Fe to S led to the preferential formation of the FeN_4S_2 structure during pyrolysis, whereas Co/Ni directly coordinated with single S atoms in the post-pyrolysis active sites [Figure 2F]. FeN_4S_2 exhibited superior ORR catalytic performance compared to Co/NiN_3S_1, which can be attributed to the higher charge density in the Fe center generated by the increment of S doping. However, this prompts inquiries regarding the dosage of dopants. Theoretically, the number and positioning of the doped atoms in the second shell matter as well, as the structural asymmetry affects charge depletion and accumulation to varying degrees, improving electron transport process[27]. In the research of Chang *et al.*, double P doping generated excessive electron transfer from Fe/P to N species than single P doping [Figure 2G and H],

resulting in stronger adsorption of OH*, which was unfavorable for the ORR process[28]. As for structural distortions and local strain induced by mismatching of atomic radius[29], however, the lack of accurate synthesis and characterization methods has limited research into the mechanism of strain effect as a result of different numbers and positions of dopants, necessitating further exploration.

Designing atoms in the higher shell

As the distance between introduced atomic entities and the active metal center increases, the level of interaction gradually diminishes. However, the so-called long-range interaction from the distant shells still exerts a significant impact on the reactivity of MN_4 sites. From this perspective, one can design not only dispersed heteroatoms to facilitate electron transfer through the electronic "pull effect"[30], but also additional atomic sites to function as an electroactivity modulator or generate synergistic effect[31]. The former, apart from emphasizing the disruption of charge symmetry at single atomic sites[32], necessitates acknowledging the coordination field effects induced by light heteroatoms from higher shells. Yin *et al.* revealed heteroatom-driven cerium single-atom stabilization[33]. The long-range interaction of P and S sites enhances the electroactivity and site-to-site electron transfer while N stabilizes the Ce single atoms to form CeN_4 sites. And the electronic modulation through the coordination field can be reflected in projected density of states (PDOS). It can be seen in Figure 3A and B that the incorporation of P and S guarantees the highest electroactivity and alleviates the electron transfer barrier with a proper ratio. Furthermore, the microenvironment of outer coordination shells was engineered by Li *et al.* through ternary heteroatomic doping[34]. At low iron loading (≈0.89 wt.%), N, F, S triple-doped hollow carbon nanofibers endow individual FeN_4 site with high intrinsic activity, resulting in a remarkable ORR half-wave potential (0.90 V) in alkaline media. Therefore, coupling single-atom metal sites with a complex coordination environment is a promising approach to improve electronic mobility. Besides, single atomization of rare earth elements induced by heteroatomic coordination field broadens the boundaries of the ORR catalytic system.

In terms of newly introduced atomic sites, the effect extends from the improvement of electron transfer to site interaction, and it prompts the exploration of appropriate spatial distance between interactional sites. Sun *et al.* built CuN_4 surrounding with Se_1C_3 atomic sites and an optimal distance between Cu and Se was deemed to be 3.64 Å, which presented the least ORR overpotential than other distances [Figure 3C][35]. In this case, the synergistic catalytic path from OOH* in Cu_1N_4 to O* in Se_1C_2 could be regulated to the best [Figure 3D], corresponding to its outstanding performance. Similar trend in the existence of optimal distance between modulating atomic entities and the original active center was discovered in other research[36]. This puts forward higher requirements for accurate chemical synthesis methods. Furthermore, the synergy of site interaction might induce the bifunctional catalytic capability, which is highly desired for energy storage and conversion systems[37,38]. For instance, CoN_4 and NiN_4 sites were anchored adjacent to FeN_4 for bifunctional oxygen electrocatalysis. Liu *et al.* discovered that CoN_4 could optimize the ORR performance at FeN_4 sites while exhibiting oxygen evolution reaction (OER) activity [Figure 3E][39]. By manipulating the configuration of bimetallic sites, the optimal adsorption of *O could be achieved, which attained both minimum overpotential for both ORR at Fe sites and OER at Co sites [Figure 3F and G]. The bifunctional oxygen electrocatalysis displayed a small potential gap (ΔE) of 0.79 V, indicating its superior catalytic bifunctionality and electrode reversibility. Chen *et al.* constructed atomically dispersed Fe and Ni sides on the different sides of the hollow carbon nanosphere[40]. Similarly, FeN_4 on the outer surface contributed to ORR activity and NiN_4 on the inner surface is responsible for the OER process, respectively. These observations demonstrate the generation of multifunctional catalytic ability originates from the synergistic effect between the introduced single metal sites and ORR active centers. By fine-tuning the local structure or spatial orientation of bimetallic sites, both optimized ORR and OER activity can be achieved.

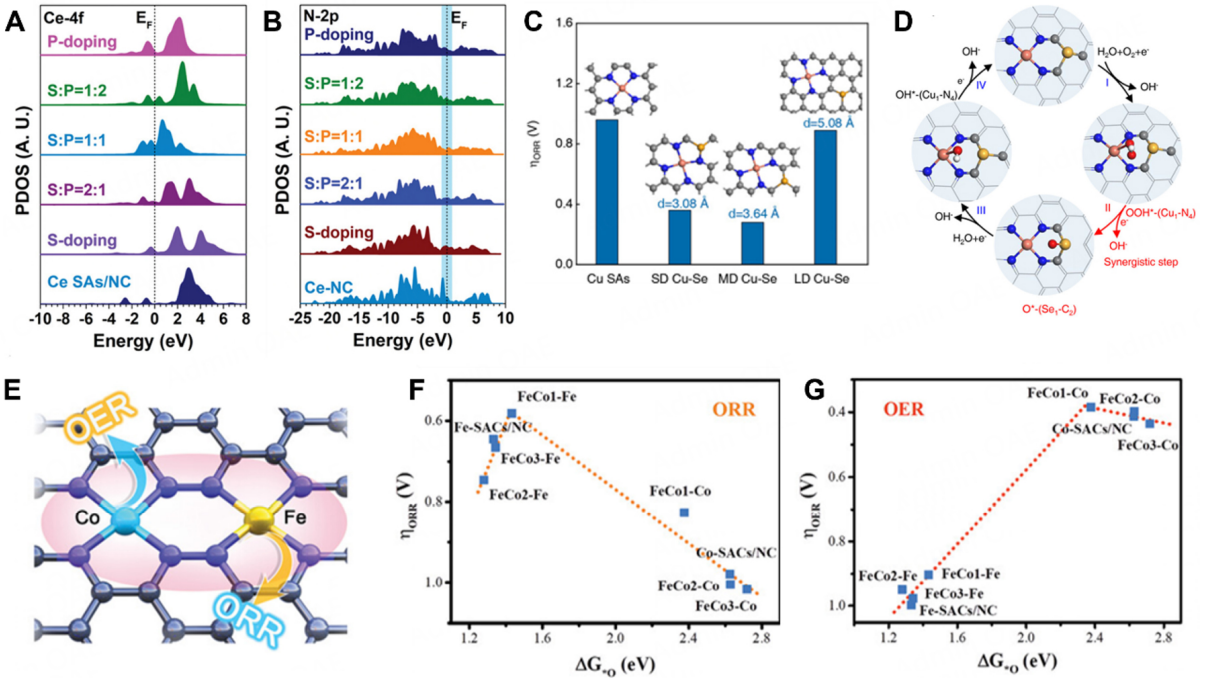

Figure 3. PDOS of Ce-4f (A) and N-2p (B) with different S:P ratios in the coordination environment. Reproduced with permission[33]. Copyright 2023, John Wiley and Sons. (C) η_{ORR} on CuN_4 and Cu-Se pairs with varied distances. Reproduced with permission[35]. Copyright 2023, John Wiley and Sons. (D) The calculated ORR reaction paths for medium-distance Cu-Se pair. Reproduced with permission[35]. Copyright 2023, John Wiley and Sons. (E) Schematic of Fe-Co pair with bifunctional catalytic capability. Reproduced with permission[39]. Copyright 2022, John Wiley and Sons. Volcano plots of ORR (F) and OER (G) for varied configurations of Fe-Co pairs. Reproduced with permission[39]. Copyright 2022, John Wiley and Sons.

Adjusting the intrinsic order

Apart from engineering microenvironment of MN_4 through introducing atomic entities in the outer shells, intrinsic order of atoms also emerges as a pivotal factor to regulate the inherent nature of active sites[41,42]. In the scope of M-N-C catalysts, intrinsic order is constructed by N and C atoms on the support with various heterocyclic structures, typically, i.e., the pyrrolic-, pyridinic-, and graphitic-N [Figure 4A]. Exploring the contribution of different N types to active sites is crucial for unraveling structure-performance relationships in M-N-C catalysts. And the current discourse primarily revolves around the discrepancy of MN_4C_{12} (pyrrole-type) and MN_4C_{10} (pyridine-type) as the origin of ORR activity[7,43-47]. Ni *et al.* attributed active sites in Fe-N-C catalysts to the iron center with pyrrolic N-coordination[48]. Employing operando Mössbauer spectroscopy, ORR intermediates attached to FeN_4C_{12} were detected rigorously by distinct isomer shift δ_{iso} and quadrupole splitting ΔE_Q [Figure 4B]. It was thereafter validated computationally by Hu *et al.* through constant-potential implicit solvent models that pyrrolic N contributes to a higher activity[49]. Besides, pH-dependence of active sites was interpreted as the variation in the affinity of the adsorbed species. As shown in [Figure 4C], pyridinic FeN_4 adsorbed OH* too strongly at the high pH and low potential location while the alkaline environment further hindered the desorption process of OH*, indicating its inferior performance in alkali conditions. On the other hand, the rate-determining step for pyrrolic FeN_4 underwent a transit from OH* desorption to O* protonation as pH increases, and pyrrolic FeN_4 exhibited a more optimized adsorption strength for ORR intermediates across a wide potential range [Figure 4D]. Therefore, design for activity improvement for M-N-C should be aimed at increasing the content of pyrrolic N with promoted O* protonation in the alkaline and facilitated OH* desorption in the acid based on the above observations.

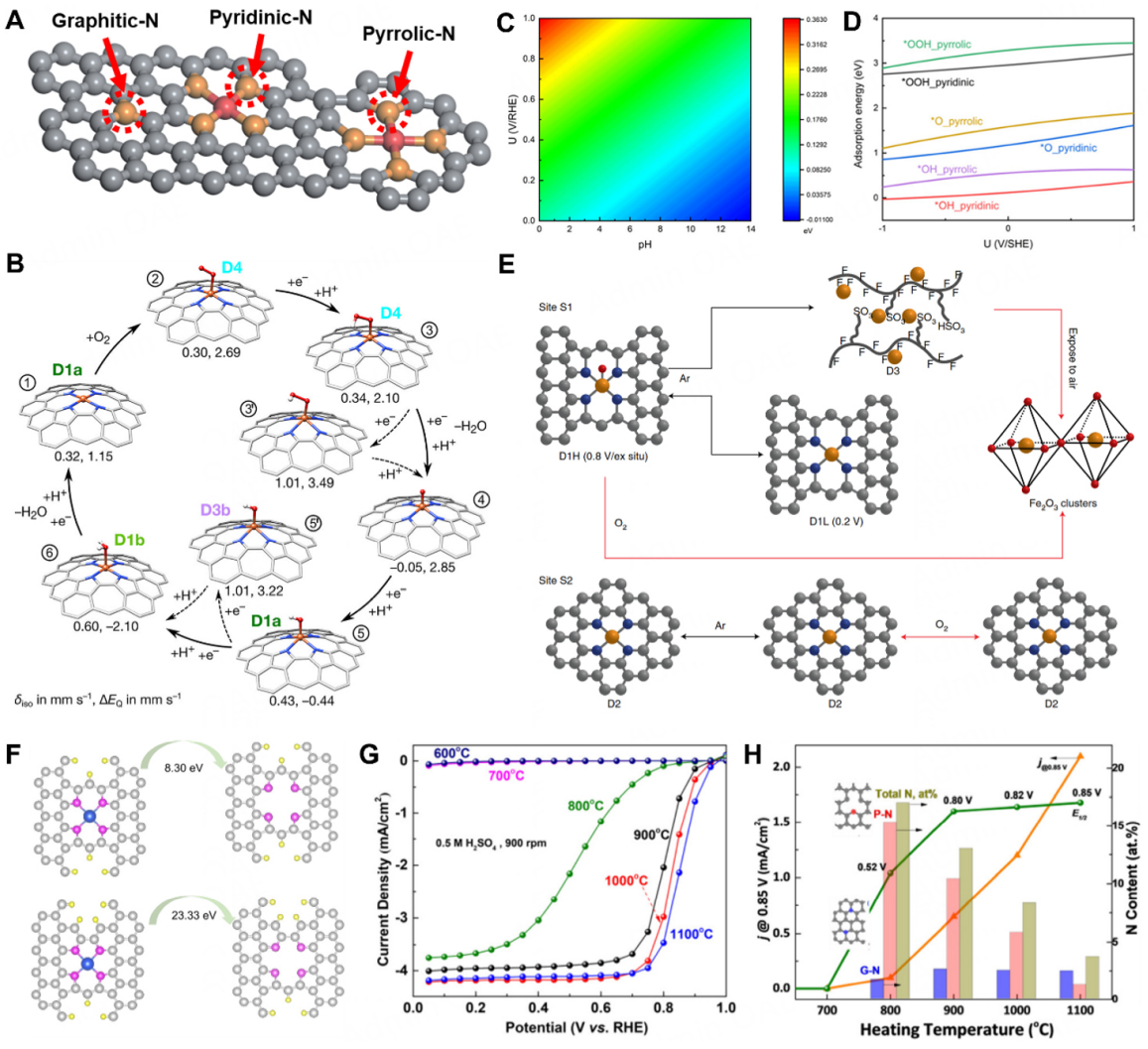

Figure 4. (A) Schematic illustration of pyrrolic-, pyridinic- and graphitic-N on the carbon support. (B) Identification of ORR intermediates adsorbed on pyrrole-type active sites derived from Mössbauer spectroscopy. Reproduced with permission[48]. Copyright 2022, American Chemical Society. (C) Contour plot showing adsorption energy of OH* on pyridinic FeN_4 sites as a function of pH and potential. Reproduced with permission[49]. Copyright 2022, American Chemical Society. (D) Comparison of adsorption energy of ORR intermediates between pyrrole-type and pyridine-type active sites. Reproduced with permission[49]. (E) Coordination or structural changes of pyrrole-type and pyridine-type active sites under operando conditions. Reproduced with permission[53]. Copyright 2020, Springer Nature. (F) Comparison of ΔG of demetallation between pyrrolic FeN_4 and monosymmetric FeN_2 + N'_2. Reproduced with permission[55]. (G) ORR activity of Fe-N-C catalysts prepared at different temperatures (600-1,100 °C). Reproduced with permission[57]. Copyright 2017, American Chemical Society. (H) Correlation between ORR activity and content of varied types of nitrogen altered with temperature. Reproduced with permission[57]. Copyright 2017, American Chemical Society.

For the construction of intrinsic order, it is imperative to not only consider the electroactivity but also prioritize long-term durability, since the severe activity loss of M-N-C catalysts (particularly in the acidic environment) limits their large-scale application in electrochemical devices[50]. Meanwhile, the trade-off between activity and stability remains a conundrum for M-N-C active site design[51,52]. The more intrinsically active pyrrolic FeN_4 sites, however, are prone to deactivate during fuel cell operation, as identified by Li *et al.*[53]. During ORR process, FeN_4C_{12} converted to inactive ferric oxides rapidly and irreversibly whereas FeN_4C_{10} was more stable against demetallation and contributed to long-term durability [Figure 4E]. In view of this, pyridine-type active sites are preferred, and Liu *et al.* developed an effective approach for active site conversion[54]. Depositing a layer of nitrogen-carbon coating, the defect-rich pyrrolic-N coordinated sites

spontaneously transformed into highly stable but less active pyridinic-N coordinated sites during the pyrolysis process. The as-converted catalysts displayed an encouraging stability improvement under the accelerated stress test (124 mV loss to 17 mV loss in $E_{1/2}$) and long-term steady-state test (80% loss after 200 h to 13% loss after 319 h). In addition, Bai *et al.* discovered novel active sites with monosymmetric structure via chemical vapor modification as well[55]. FeN_2 + N'_2 encompassing pyrrolic-N and pyridinic-N at each side not only weakened OH* bonding, but also impeded demetallation process significantly [Figure 4F]. The prominent enhancement in structural stability led to negligible decay after 200,000 cycles and sustainable operation of fuel cells over 248 h at 0.65 V.

Graphitic-N dispersed in the outer coordination shells, on the other hand, affects the single-atom active center akin to doped heteroatoms. Owing to a larger electronegativity than C, graphitic-N in the carbon sheet could induce electron deficiency in neighboring carbon atoms and reduce the energy gap between the Fermi level and conduction band, thereby enhancing the charge mobility of the graphene lattice[56]. Typically, the content of graphitic-N increases as the pyrolysis temperature elevates, and Zhang *et al.* attributed the additional improved performance from 900 to 1,100 °C to the contribution of graphitic-N [Figure 4G], since the increment of N doping resulted in a nonuniform electron distribution[57]. However, it should be noted that the total N content diminished with dramatically augmented graphitic-N *vs.* coordinated-N ratio [Figure 4H], and thus, it is essential to provide a sufficient amount of N source for the effective anchoring of atomically dispersed metal. Moreover, graphitic-N might give rise to the higher selection of $2e^-$ process[58], which is undesired for the electrochemical conversion system.

INTRODUCING METALLIC SPECIES BEYOND THE FIRST COORDINATION SHELL

Introducing metallic species in proximity to MN_4 sites is another emerging regulation method, which can effectively ameliorate the ORR performance of M-N-C. It should be noted that metallic species encompass metal nanoparticles and metal nanoclusters, ranging from a few atoms to hundreds or thousands of atoms. The scale effect leads to significant disparities in the geometry and electronic structure of nanoclusters and nanoparticles, resulting in a distinct interaction with single atomic sites[59]. In this section, we emphasize the modification of the electronic structure of MN_4 by nanoclusters and the function of the nanoparticles as site stabilizers for alleviating deactivation of catalytic sites.

Incorporating nanoclusters as electronic modulator

The electronic structure of atomically dispersed metal atoms can be regulated through coupling with nanoclusters. Recently, the ORR performance of M-N-C has been enhanced by utilizing various types of clusters, including pure metal clusters[60-62], metallic carbides[63,64], nanoalloys[65,66], *etc.* For example, Wang *et al.* revealed the importance of Pt nanoclusters for the enhancement of PtN_4 ORR activity through rigorous calculations[67]. By evaluating PtN_4, Pt nanoclusters individually, and their combination, it is observed that the Pt single atomic sites modified by Pt nanoclusters exhibit a moderate Bard charge [Figure 5A]. This signifies its favorable adsorption energy towards ORR intermediates, ensuring efficient adsorption of a substantial quantity of intermediates without impeding the desorption process. The Gibbs free energy diagram illustrates the manifestation of the lowest energy barrier for the $4e^-$ ORR reaction [Figure 5B], thereby providing further evidence for the efficacy of nanoclusters in modulating the electronic structure of single atoms. Additionally, other pure metal clusters such as iron[68], cobalt[69], copper[62], and manganese[70] have also demonstrated the ability to enhance the catalytic properties of M-N-C for ORR. Fe_7 nanoclusters were constructed by Wang *et al.* near the FeN_4 site on multichannel porous carbon fibers, leading to an augmentation in the total state of density, which facilitated electron transfer during ORR process [Figure 5C][61]. And the subsequent PDOS calculations revealed a significant alteration in the 3d energy level of Fe in FeN_4 site induced by Fe_7 nanoclusters, thereby optimizing the hybridization between Fe

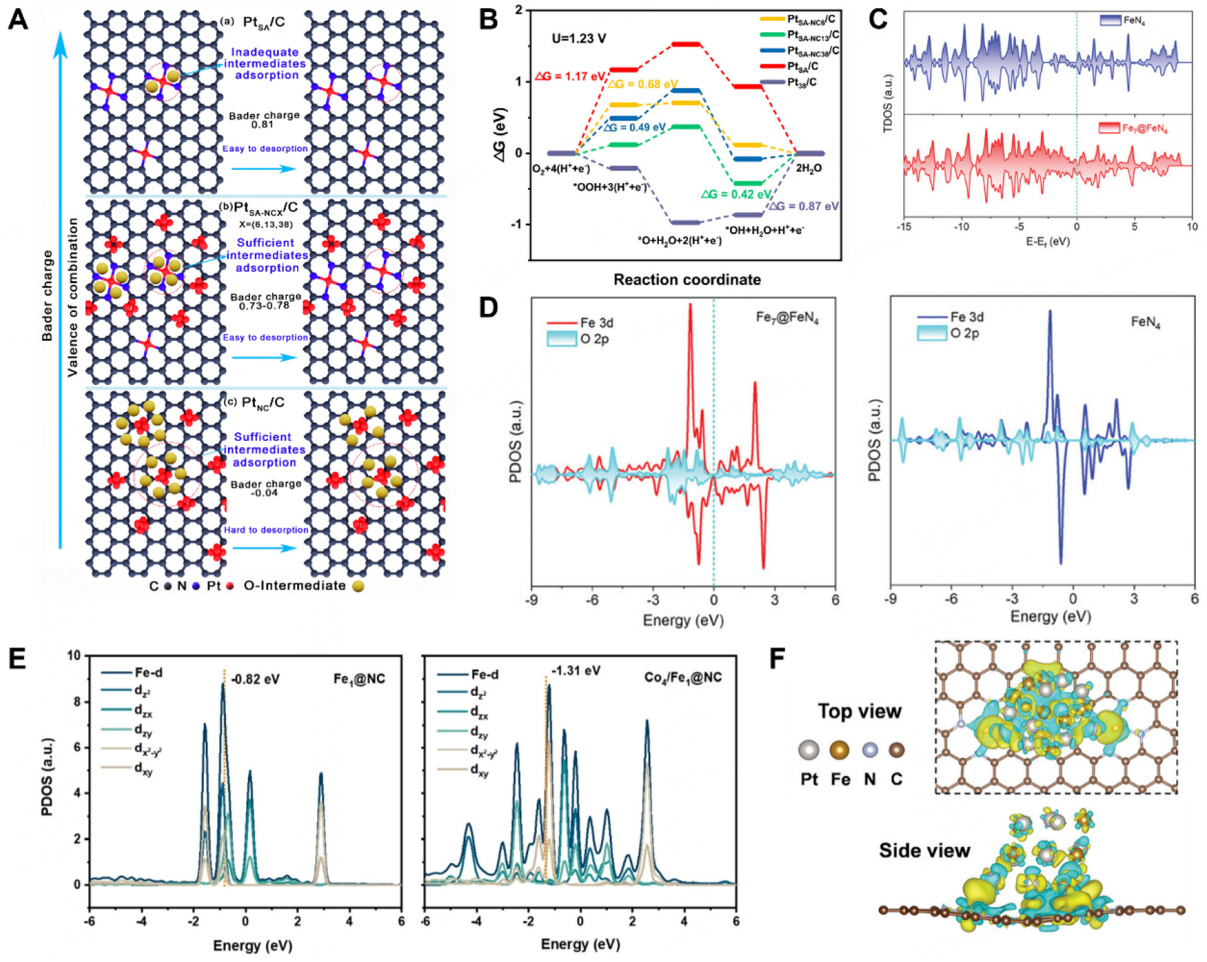

Figure 5. (A) Schematic depiction of the catalytic function of PtN_4, PtN_4@Pt nanoclusters and Pt nanoclusters in the ORR process. Reproduced with permission[67]. Copyright 2024, American Chemical Society. (B) ORR free energy diagrams for PtN_4 (redline), PtN_4@Pt_6 nanoclusters (yellow line), PtN_4@Pt_{13} nanoclusters (green line), PtN_4@Pt_{38} nanoclusters (blue line), and Pt nanoclusters (black line) at U = 0.9 and U = 1.23 V along 4e$^-$ pathway. Reproduced with permission[67]. Copyright 2024, American Chemical Society. (C) Total state of density of FeN_4 and FeN_4@Fe_7 nanoclusters. Reproduced with permission[61]. Copyright 2024, John Wiley and Sons. (D) Projected density of states of FeN_4@Fe_7 nanoclusters and FeN_4. Reproduced with permission[61]. Copyright 2024, John Wiley and Sons. (E) Projected density of states of FeN_4 and FeN_4@Co_4 nanoclusters on the d-band of Fe-N_4 site. Reproduced with permission[69]. Copyright 2024, John Wiley and Sons. (F) The results of calculated charge density difference for FeN_4@PtFe nanoalloys. Yellow area: electrostatic charge density is positive; cyan area: electrostatic charge density is negative. Reproduced with permission[66]. Copyright 2024, John Wiley and Sons.

3d orbital and oxygen p orbital [Figure 5D]. Besides, Han *et al.* designed homogeneous Co_4/Fe_1 polymetallic active sites using "pre-constrained" strategy"[69]. Through the coupling of Co_4 nanoclusters, there is a perceptible downward shift in the d-band center of Fe atoms, which weakens their bonding strength with O* and enhances the activity of ORR [Figure 5E].

In addition to pure metal clusters, the electronic structure of M-N-C can also be influenced by metallic carbides[71-73] and nanoalloys[66] in a similar manner. The incorporation of Fe/Fe_3C nanocrystals was observed to significantly enhance the ORR performance of FeN_4[72]. Afterward, many studies have further investigated the synergistic effects of Fe_3C nanoclusters on the electronic structure of FeN_4 sites[74,75], and have been extended to different systems, such as FeN_4@Ti_3C_2[76], FeN_4@Fe_4C[71], MnN_4@Fe_3C[77], *etc.* Chang *et al.* utilized the seed-mediated strategy to fabricate Fe_3C species that are closely surrounded by Fe-N_4-C active

sites[64]. By slightly adjusting the proportion of components, the optimal electrical interaction between Fe_3C and FeN_4 was achieved. Xu *et al.* synthesized a doped carbon skeleton with a unique structure via g-C_3N_4-assisted growing strategy, consisting of 1D nanotubes and 2D nanosheets[78]. FeN_4 active sites coupled with Fe_3C encapsulated in this hierarchical structure, which promoted both mass and electron transfer, demonstrated a strong synergistic effect and accelerated the oxygen adsorption kinetics. In addition, the utilization of nanoalloys is also a potent strategy for the modification of M-N-C. Wu *et al.* uniformly deposited PtFe nanoalloys onto the surface of FeN_4 sites, where the combination of both acted as an electronic structure modulator[66]. As shown in Figure 5F, the differential charge density calculations reveal a notable accumulation of charges between FeN_4 sites and PtFe nanoalloys, suggesting the presence of reciprocal electron transfer and electron modulation between them. The study conducted by Zhu *et al.* investigated the synergistic effects of CoFe nanoalloys and MN_4, encompassing a comprehensive evaluation ranging from material design and simulation analysis to fuel cell application[65]. In summary, the assistance of neighboring metal clusters is conducive to enhancing the kinetics and thermodynamics of ORR at single atomic sites, as supported by both experimental and theoretical evidence. In contrast with isolated single atomic sites, modification by nanoclusters fine-tunes the adsorption/desorption energy of oxygen intermediates through the optimization the electron structure of the catalytic active center, thereby achieving superior ORR performance.

Incorporating nanoparticles as site stabilizer

As electronic structure of MN_4 can be effectively regulated with assistance of nanoclusters, the stability and durability of M-N-C towards ORR, despite significant advancements in their activity, remains insufficient, particularly in the acidic environment[79,80]. Currently, the degradation mechanism is commonly believed to vary under different pH conditions[81]. In an acidic environment with relatively poor stability, MN_4 site is susceptible to trigger Fenton or Fenton-like reaction with hydrogen peroxide (H_2O_2) during the 2-electron process[80,82,83]. The carbon matrix of catalysts could be irreversibly damaged by the aggressive reactive oxygen species (ROS), particularly hydroxyl radicals (·OH)[84]. On the other hand, in alkaline environments, the metal leaching from active sites during the ORR process becomes an inevitable factor contributing to activity decay and serves as the primary degradation mechanism. Therefore, it is imperative to eliminate ROS generated by side reaction and decelerate the leaching of metal ions to pursue superior ORR performance. As aforesaid, designing the intrinsic order enhances inherent resistance against degradation, while the incorporation of nanoparticles can function as site stabilizers from the outer coordination environment.

Introduction of radical scavengers into the carbon support is an effective strategy for enhancing the stability of ORR catalysts by rapidly eliminating ROS generated during the ORR process, and thus inhibiting Fenton or Fenton-like reactions. The functionality of radical scavenging has been well-recognized in nanoparticles, especially metal oxide nanoparticles[85,86]. Xie *et al.* employed the high-temperature pulse technique to synthesize Ta-TiO_x modulating Fe-N-C catalysts[87]. Qualifying with a highly efficient capacity to scavenge oxygen radicals, dispersing Ta-TiO_x nanoparticles throughout the carbon framework can effectively decelerate the attack of free radicals on the active site during the ORR process [Figure 6A]. Further DFT calculations proved that TaO_2-OH had a higher affinity towards H_2O_2 and related radicals [Figure 6B], thereby preventing the destruction of active sites in Fe-N-C through competitive adsorption. The protected catalyst exhibited exceptional durability, which showed a current density decay of only 3% at 0.9 V after an accelerated durability test, whereas Fe-N-C alone decayed by 33% [Figure 6C]. In addition, cerium dioxide (CeO_2) has also been found to be a proficient scavenger of free radicals[88,89]. ROS formed at MN_4 sites, such as ·OH and HO_2·, can be rapidly captured and eliminated by CeO_2 nanoparticles. Increasing the dispersion and reducing the size of the nanoparticles is important because scavengers adjacent to the catalytic active sites can simultaneously eliminate the generated ROS, thereby reducing the survival time of radicals and

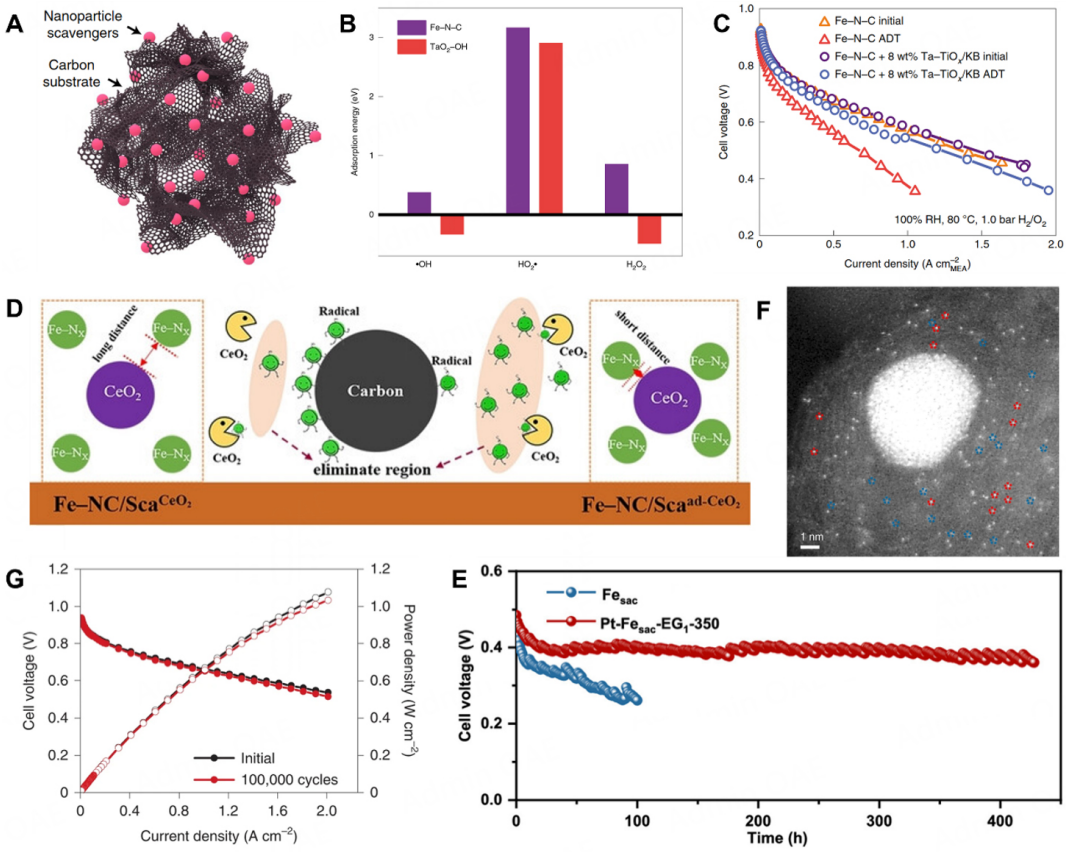

Figure 6. (A) Schematic illustration of carbon substrate well-dispersing with nanoparticle scavengers. Reproduced with permission[87]. Copyright 2022, Springer Nature. (B) The size distribution of the Ta-TiO_x nanoparticles. Reproduced with permission[87]. Copyright 2022, Springer Nature. (C) Adsorption affinity of H_2O_2 and derived free radical on the Fe-N-C and TaO_2-OH surfaces. Copyright 2022, Springer Nature. Reproduced with permission[87]. (D) Schematic depiction of CeO_2 nanoparticles scavenging radicals and their elimination zone. Reproduced with permission[89]. Copyright 2023, John Wiley and Sons. (E) Long-term stability test of FeN_4 with Pt nanoparticles at a constant current density of 0.1 A cm^{-2}. Reproduced with permission[90]. Copyright 2023, American Chemical Society. (F) HAADF-STEM image of atomically dispersed Pt, Fe sites and Pt-Fe alloy nanoparticles. Reproduced with permission[93]. Copyright 2022, Springer Nature. (G) H_2/O_2 fuel cell polarization and power density plots of the Pt-Fe-N-C with Pt-Fe nanoalloys before and after 100,000 potential cycles between 0.6 and 0.95 V. Reproduced with permission[93]. Copyright 2022, Springer Nature.

limiting the spatial extent of their damaging effects [Figure 6D]. To sum up, the stability of ORR in M-N-C can be significantly improved with the modification of radical scavengers. This strategy extends the protection of M-N-C from passive shielding to active defense.

Instead of acting as radical scavengers, nanoparticles can also strengthen M-N bonds through electronic interaction to prohibit demetallation. Gao *et al.* investigated the impact of different types, forms, and contents of metal nanoparticles on M-N bond strength[90]. The underlying mechanism goes that nanoparticles, acting as electron donors, can augment the electron density of the MN_4 site, thereby enhancing the M-N bond and impeding metal dissolution. In their work, Fe-N-C@Pt nanoparticles were found to be the most stable among all synthesized M-N-C materials and in the direct methanol fuel cell stability test, the cell voltage experienced a rapid decrease in the first 10 h and then remained stable in subsequent 430 h, which excess most of the ORR catalysts nowadays [Figure 6E]. Pt species are consequently deemed to be an excellent stabilizer for single-atom metal sites[91,92]. Furthermore, in Xiao's research, the stability of Fe-N-C was improved greatly after hybridization with Pt single atoms and Pt-Fe alloy nanoparticles[93]. The simultaneous presence of dispersed single atoms and nanoparticles was distinctly

observed in high-angle annular dark-field scanning transmission electron microscopy (HAADF-STEM) [Figure 6F]. Synergistic effects among active sites in hybrid electrocatalysts effectively hindered the dissolution of iron, thus mitigating the degradation of membranes and ionomers in fuel cells. As a result, 97% activity retention was achieved after 100,000 potential cycles [Figure 6G].

TAILORING NON-METALLIC MODULATORS BEYOND THE FIRST COORDINATION SHELL

Defects and functional groups are inevitable formation components during the synthesis process of heterogenous catalysts, and the development of precise design strategies to augment the active sites merits comprehensive investigation. Atomic defects facilitate the electron mobility and the accessibility between MN_4 sites and reactants, which is advantageous for accelerative mass transfer and reduced internal ohmic resistance[94,95]. Additionally, functional groups can be constructed purposely and systematically to explore the favored active sites associated with specific local states[96]. Through meticulous design of these non-metallic modulators, it is plausible to optimize the electronic structure of the single-atom active sites.

Atomic defect modification

The significance of defects in improving catalytic efficiency is well-recognized. Vacancies are a common kind of defect in carbon-based materials[97]. These coordination vacancies can modulate the electronic structure from the higher coordination shell, thereby optimizing the behavior of reactive intermediates. Significant focus has been placed on enhancing the efficiency of M-N-C catalysts for ORR through optimized atomic vacancies, including Fe-N-C with carbon vacancies[54], Zn-N-C with nitrogen vacancies[98], Co-N-C with carbon vacancies[99], and so on. Specifically, M-N-C with atomic-level carbon vacancies (M=Fe, Co, Ni, Cu, and Mn) was synthesized by Tian *et al.*, aiming to precisely control the chemical environment and electronic configuration of the metal center[100]. Fe-N-C with well-defined electronic structure exhibited superior ORR activity and stability compared with commercial Pt/C and other reference samples. To further explain the reason, the authors considered six possible single carbon vacancies, as shown in Figure 7A. By calculating the Gibbs free energy change on the defective FeN_4 along the 4e ORR process, site E with a carbon vacancy in the fourth coordination shell was found to be most conducive to the process of the potential-determining step, that is, the reduction of OH* [Figure 7B]. Liu *et al.* further investigated the effect of divacancy carbon defects on FeN_4 sites[101]. The 6 (5-8-5), 6a (555-777), and 6I (5-7-7-5) models were highlighted due to their modification with good thermodynamic stability [Figure 7C]. The influence of adjacent divacancy resulted in a decrease in the O_2 adsorption energy while altering the bond length, such as O-O bond elongation and Fe-O bond shortening [Figure 7D]. These results suggest that introducing carbon vacancy in the high coordination layer optimizes the interaction between FeN_4 sites and oxygen species, thereby contributing to better ORR performance.

The edge-site engineering of MN_4 site has also aroused intensive research[102-104]. Reconfigured by the mesoporous structure, the MN_4 moiety located at the edge exhibited a favorable energy profile thermodynamically compared to the intact atomic configuration, leading to enhanced catalytic performance[105]. Besides, the design based on the edge increases the accessibility and the loading of MN_4 sites[102]. Cui *et al.* constructed edge-rich single-atomic Cu-N_4 sites by NH_4Cl-assisted etching strategy[106]. The introduced NH_4Cl promoted the formation of abundant carbon edge, which was preferential for the anchoring of Cu sites. Impressively, the as-synthesized Cu-N-C exhibited a high $E_{1/2}$ of 0.91 V [*vs.* reversible hydrogen electrode (RHE)] and onset potential of 1.02 V (*vs.* RHE), respectively, surpassing the Pt/C benchmark and ranking among the top-performing electrocatalysts. Wang *et al.* further demonstrated the electron redistribution of edge sites in defective carbon[102]. According to DFT calculations, FeN_4 anchored at the edge exhibited a higher electron density, indicating greater electron donor capacity than those anchored on the intact carbon basal plane. And a narrower highest-occupied molecular orbital (HOMO)-lowest-

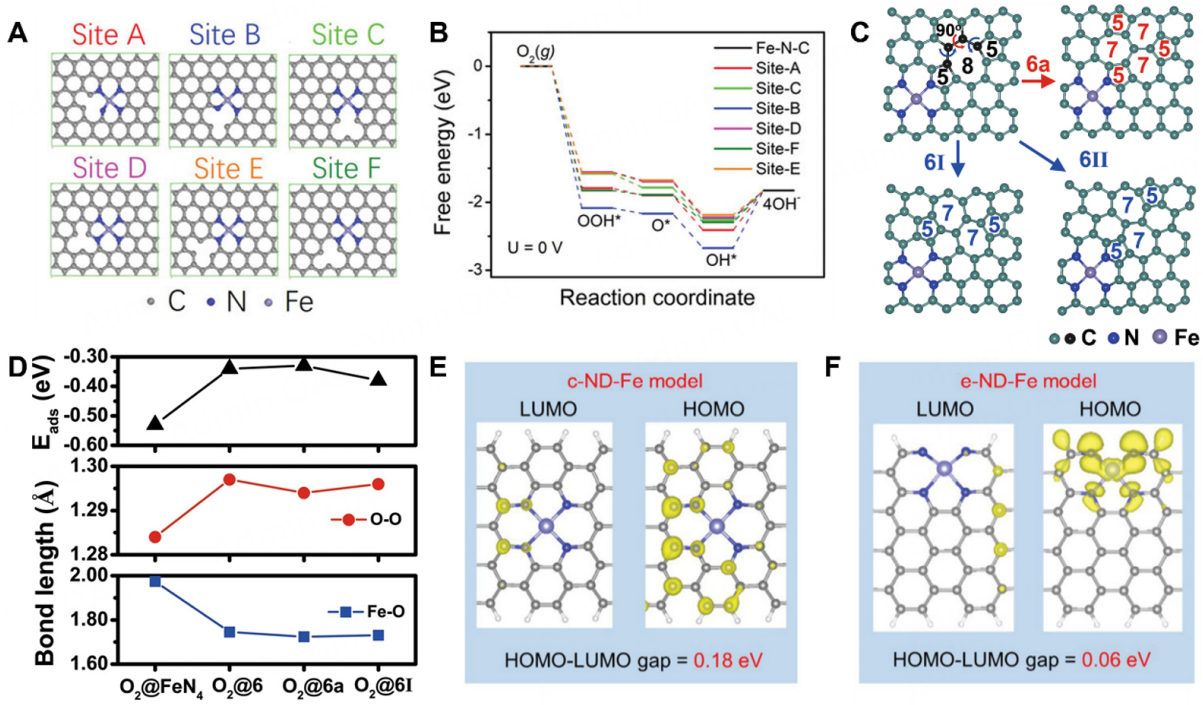

Figure 7. (A) The atomic structures of FeN_4 with six single carbon vacancies. Reproduced with permission[100]. Copyright 2023, John Wiley and Sons. (B) The free energy diagrams of ORR on FeN_4 with six single carbon vacancies. Reproduced with permission[100]. Copyright 2023, John Wiley and Sons. (C) Variants of FeN_4 with different divacancy defect models. Reproduced with permission[101]. Copyright 2022, Springer Nature. (D) Adsorption energy of O_2, O-O, and Fe-O bond length on FeN_4 with different divacancy structures. Reproduced with permission[101]. Copyright 2022, Springer Nature. HOMO and LUMO distributions of the center-N-modified divacancies trapped Fe sites (E) and edge-N-modified divacancies trapped Fe sites (F) models. Reproduced with permission[102]. Copyright 2020, John Wiley and Sons.

unoccupied molecular orbital (LUMO) gap could generate rapid electron transfer in the catalytic reactions [Figure 7E and F]. Therefore, edge-site engineering of the MN_4 site showed structural superiority, facilitating the site formation and inducing charge distribution, thereby improving the ORR performance.

Functional group modification

The modification of single atomic sites through the functional groups in the high coordination sphere is also a crucial approach for regulating the performance of ORR. The electronic structure of the catalytic sites can be systematically modulated by the electron-withdrawing or electron-donating effect imparted by functional groups, thereby effectively regulating the adsorption/desorption behavior of reaction intermediates[107]. The efficacy of the functional group modification has been well demonstrated in M-N-C catalysts, such as epoxy modifying Sb-N-C[108], Cu-N-C with carboxyl groups[109], hydroxyl-rich Co-N-C[110], *etc*. Recently, Wei *et al.* explored the influence of the functional group and local structure on the electronic properties of Co centers[111]. Planar conjugated structures with different functional groups [amino ($-NH_2$), hydroxyl (-OH), and sulfhydryl (-SH)] were used as the skeleton. And it is noteworthy that a higher magnetic moment (1.12 μ_B) was observed when Co site bridged triphenylene with hydroxyl functional group, indicating a transition from low-spin to high-spin states for electron filling of e_g orbitals [Figure 8A and B]. The alteration of spin states contributed to better ORR performance. Furthermore, the presence of the hydroxyl group enhanced the bonding interaction between Co and OH*, while the triphenylene skeleton contributed to a moderate integrated crystal orbital Hamilton population (ICOHP) value for medium OH* adsorption [Figure 8C]. The results profoundly disclosed the effectiveness of functional group modification on the electronic state of metal centers. Additionally, the effect of

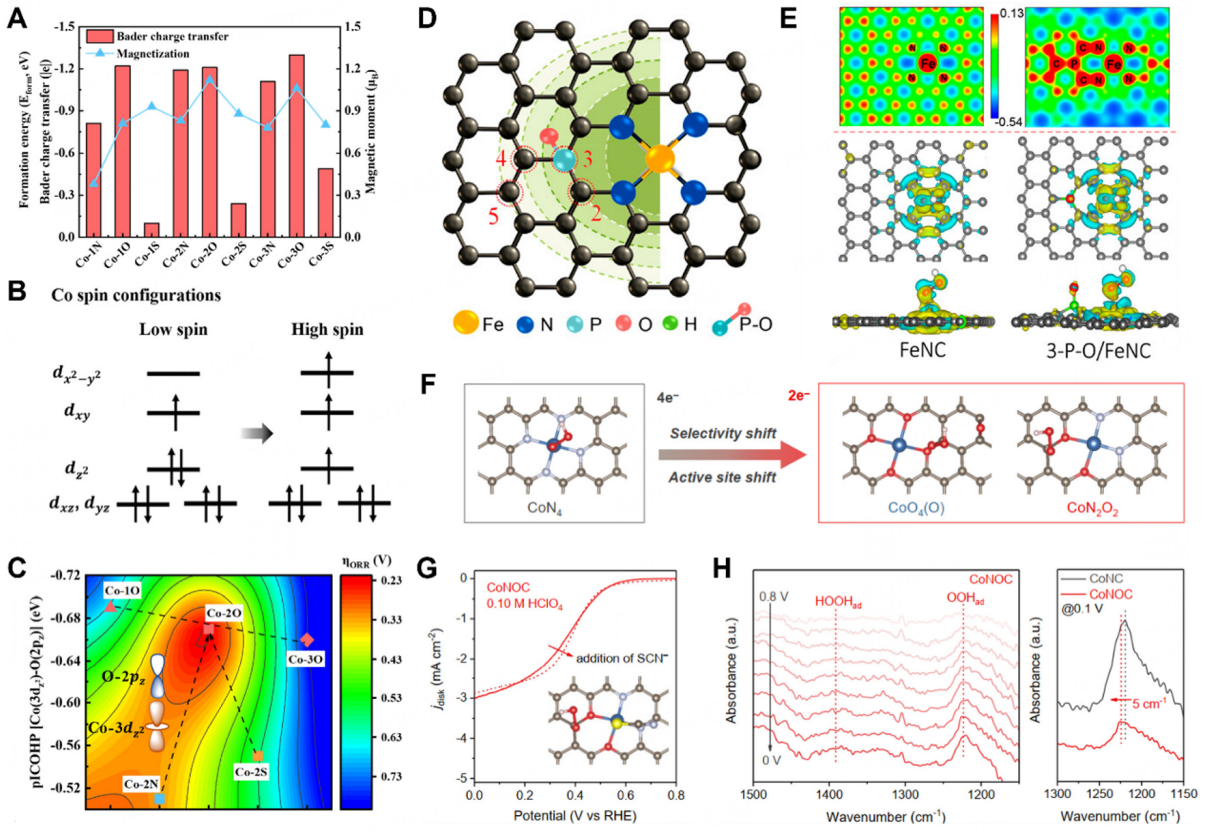

Figure 8. (A) Bader charge transfer and magnetic moments of Co sites coupled with different local structures. Reproduced with permission[111]. Copyright 2023, American Chemical Society. (B) Reconfiguration of spin state in the Co center with a high magnetic moment. Reproduced with permission[111]. Copyright 2023, American Chemical Society. (C) 2D volcano plot of η_{ORR} *vs.* ICOHP of Co-O bonds between Co sites and OH* species. Reproduced with permission[111]. Copyright 2023, American Chemical Society. (D) Schematic diagram of FeN_4 with P-O bond in different outer shells. Reproduced with permission[112]. Copyright 2023, American Chemical Society. (E) Top: Contour plots showing the charge density difference after *OOH adsorption; bottom: differential charge densities upon *OOH adsorption. Reproduced with permission[112]. Copyright 2023, American Chemical Society. (F) Schematic illustration of selectivity shift and active site shift after the decoration of C-O-C groups. Reproduced with permission[113]. Copyright 2021, American Chemical Society. (G) LSV curves for Co-N-C with C-O-C groups before and after the addition of 10 mM KSCN. Reproduced with permission[113]. Copyright 2021, American Chemical Society. (H)*In situ* ATR-SEIRAS spectra of Co-N-C with C-O-C groups and the comparison of the band around 1220 cm^{-1} for Co-N-C with C-O-C groups and Co-N-C. Reproduced with permission[113]. Copyright 2021, American Chemical Society.

incorporating a solitary functional group into a specific coordination layer has been investigated in other studies. Liu *et al.* introduced P-O bonds in the third coordination shell of the catalytic active center to regulate the electronic structure of the FeN_4 sites [Figure 8D][112]. The doping of P-O bonds induced an asymmetric distribution of charge density, resulting in a larger electron transfer and concentrated electron depletion on the Fe center [Figure 8E]. Tang *et al.* modified the first and second coordination spheres of the Co catalytic center simultaneously to discover the structure-property relationship[113]. Interestingly, the transfer of the catalytic active center occurred after the functional group of the second Co coordination sphere [Figure 8F], which led to a change in the selectivity of ORR from the $4e^-$ process to the $2e^-$ process. The authors employed thiocyanide (SCN^-) poisoning as a means of validating the shift in active sites [Figure 8G]. And *in situ* attenuated total reflectance surface-enhanced infrared absorption spectroscopy (ATR-SEIRAS) proved that Co-N-C with C-O-C groups exhibited a readily identifiable $HOOH_{ad}$ band and the OOH_{ad} band with weaker intensity, revealing the origin of selectivity toward the $2e^-$ ORR [Figure 8H]. In general, introducing functional groups through non-direct coordination can effectively adjust the electron

density of catalytic centers and has a more moderate regulatory effect than direct coordination. Based on the descriptors constructed according to the adsorption capacity of MN_4 active sites for reactants and intermediates, one can purposefully introduce electron-withdrawing or electron-donating groups to generate appropriate adsorption behavior in order to achieve lower reaction energy barriers.

CONCLUSION AND OUTLOOK

This review summarizes the methods of modulating single atomic sites beyond the first coordination shell, focusing on the effects of adjusting atomic entities, metallic and non-metallic modulators in the vicinity of MN_4. Compared to direct coordination with single atoms, regulation beyond the first coordination shell has a more moderate control scale and can produce a more optimized electronic structure through synergistic interactions. Adjusting atomic entities could give rise to unsymmetric electronic distribution of MN_4 sites and generate synergistic effects through site interaction while manipulating the intrinsic order of single atoms which can selectively control the balance between activity and stability of active sites. The incorporation of metallic species such as nanoclusters or nanoparticles significantly adjusts the electronic structure of single-atom centers, optimizing the hybridization of metal 3d orbitals with oxygen 2p orbitals, thereby reducing the reaction barrier for ORR and producing superior performance. On the other hand, the specific configuration of the MN_4 sites with the metallic species may also change the oxygen adsorption pattern (i.e., from end-on to side-on) to promote O-O bond cleavage. In addition to serving as electronic modulators, functional nanoparticles can also act as stabilizers to enhance the stability of MN_4 sites, which is reflected in rapid removal of free radicals generated during ORR process to inhibit Fenton reactions; moreover, interaction between nanoparticles and MN_4 sites can strengthen M-N bonds to avoid demetallation. Introducing non-metallic modulators into high coordination layers is also an important way to regulate MN_4 sites. Defects can increase site exposure and adjust adsorption energy for oxygen intermediates while functional groups mainly interact with MN_4 sites through electron-donating/electron-withdrawing effects. The performance of ORR electrocatalysts modified by the above methods is summarized in Table 1.

Although extensive research has been conducted on the regulation methods of M-N-C catalysts, they still encounter obstacles in achieving widespread commercial application. Therefore, we propose the following points to illustrate the future development trend of M-N-C materials.

In situ accurate design

In the realm of ORR catalysts, the advent of M-N-C represents a paradigm shift, offering a new dimension of catalytic efficiency and specificity. This review summarizes the design of modification of M-N-C beyond the first coordination shell, but achieving accurate *in situ* control remains a challenge. The meticulous approach necessitates not only innovative design, but also a profound comprehension of the microscopic atomic scale, thereby imposing exceedingly high demands on *in situ* characterization methods. Through further development of advanced characterization techniques such as *in situ* Mössbauer spectroscopy and *in situ* XAS, combined with DFT calculations, researchers can establish precise atomic-scale structure-activity relationships. This is advantageous for the *in situ* design of micro-local configurations. By manipulating the electronic and geometric structure at the atomic scale, researchers can create catalysts that are finely tuned for specific reaction steps, minimizing unwanted byproducts and maximizing energy transformation. This level of control is pivotal for the development of next-generation catalysts that can drive chemical processes with unparalleled precision.

Large-scale production

The transition from laboratory-scale production to large-scale preparation of M-N-C is a significant leap

Table 1. Summary of M-N-C ORR performance with different modifications

Regulation method	Active site	Electrolyte	E_{onset} (V *vs.* RHE)	$E_{1/2}$ (V *vs.* RHE)	Kinetic current (mA cm^{-2})	Ref.
Atomic entities	CoN_4-S_2 2nd[a]	0.1 M KOH	1.00	0.87	35.9@0.8 V	[26]
	RuN_4-S_1 2nd	0.1 M KOH	0.998	0.861	101.7@0.8 V	[21]
	FeN_4S_1-P_1 2nd	0.1 M $HClO_4$	NA	0.814	46.7@0.7 V	[22]
		0.1 M KOH	NA	0.912	60@0.85 V	
	FeN_4-P_2 2nd	0.1 M KOH	1.01	0.90	25.4@0.85 V	[27]
	FeN_4-S_1^{hs}[b]	0.1 M $HClO_4$	0.92	0.821	6.7@0.5 V	[114]
		0.1 M KOH	1.05	0.887	7.1@0.5 V	
	FeN_4-Cl_1^{hs}	0.1 M KOH	1.02	0.917	23.8@0.85 V	[32]
	CeN_4-P^{hs}-S^{hs}	0.1 M KOH	NA	0.90	81.1@0.85 V	[33]
	FeN_4@ZrN_4	0.1 M $HClO_4$	NA	0.872	43.48@0.8 V	[115]
	FeN_4@MoN_4	0.1 M $HClO_4$	0.98	0.84	23.5@0.8 V	[116]
	CuN_4@Se_1C_3	0.1 M KOH	1.12	0.905	25.6@0.85 V	[35]
	SbN_2C_2@Se_1C_2	0.1 M KOH	NA	0.865	7.424@0.85 V	[36]
	FeN_4@NiN_4	0.1 M KOH	0.93	0.83	NA	[40]
Metallic species	FeN_4@Fe_7 AC[c]	0.1 M KOH	1.02	0.894	15.91@0.85 V	[61]
	PtN_4@Pt_x AC	0.1 M $HClO_4$	NA	0.87	9@0.85 V	[67]
	CoN_4@Co_x AC	0.1 M KOH	NA	0.89	21.64@0.85 V	[117]
	FeN_4@Co_4 AC	0.5 M H_2SO_4	0.980	0.835	NA	[69]
	MnN_4@Mn_x AC	0.1 M KOH	0.97	0.90	56.44@0.85 V	[70]
	MnN_4@Fe-Mn AC	0.5 M H_2SO_4	0.89	0.79	7.27@0.7 V	[118]
		0.1 M KOH	1.00	0.90	7.71@0.7 V	
	FeN_4@Cu_x AC	0.1 M $HClO_4$	0.96	0.83	11.9@0.8 V	[62]
		0.1 M PBS	1.02	0.84	68@0.7 V	
		0.1 M KOH	1.06	0.94	145.8@0.85 V	
	FeN_4@Fe_4C AC	0.5 M H_2SO_4	NA	0.836	14.79@0.8 V	[71]
	FeN_4@Ti_3N_2 AC	0.1 M KOH	1.00	0.92	NA	[76]
	MnN_4@Pt NP[d]	0.1 M $HClO_4$	1.01	0.93	NA	[119]
	FeN_4@Fe-CeO_2 NP	0.1 M KOH	NA	0.948	35.15@0.9 V	[120]
	Pt/FeN_4@Pt-Fe NP	0.1 M $HClO_4$	NA	0.909	NA	[93]
Non-metallic species	FeN_4-CV[e]	0.5 M H_2SO_4	NA	0.915	10.3@0.9 V	[54]
	SbN_4-CV	0.1 M KOH	NA	0.905	6.74@0.9 V	[121]
	CoN_4-CV	0.1 M KOH	0.99	0.878	12.39@0.85 V	[99]
	FeN_4-NV[f]	0.1 M KOH	0.990	0.902	51.7@0.85 V	[122]
	FeN_4@P-O	0.1 M KOH	1.01	0.912	7.54@0.9 V	[112]
	FeN_4@C-O-C	0.1 M KOH	1.08	0.92	51.75@0.85 V	[24]
	FeN_4@oxidized S	0.5 M H_2SO_4	0.88	0.76	6.6@0.85 V	[123]
		0.1 M KOH	1.01	0.91	NA	
	SbN_4@C-O-C	0.1 M KOH	1.03	0.86	24@0.82 V	[108]

[a]Atoms located in the second shell; [b]atoms located in the higher shell; [c]atomic clusters; [d]nanoparticles; [e]carbon vacancy; [f]nitrogen vacancy.

toward their commercialization and practical application. This scale-up is crucial for meeting the demands of industrial processes, which require robust and consistent performance over extended periods. However, the large-scale preparation of atomically dispersed M-N-C ORR electrocatalysts remains a challenge, closely related to unavoidable thermal annealing, atom aggregation and many other issues. Recent advancements have led to the development of innovative synthesis techniques that maintain the integrity and dispersion of single atoms on various substrates[124]. By integrating these scalable approaches, the gap between the

potential and practical use of M-N-C is narrowing, setting the stage for their widespread adoption in catalysis-driven industries.

Computational high-throughput screening

High-throughput screening for electrocatalysts has emerged as a powerful tool in the discovery and optimization of M-N-C catalysts. By leveraging advanced algorithms and machine learning techniques, researchers can rapidly evaluate a vast array of potential catalyst structures and compositions. This approach also significantly accelerates the identification of promising candidates by predicting their performance and stability with various catalytic reactivity descriptors[125]. High-throughput screening not only reduces the time and cost associated with experimental trials but also provides valuable insights into the fundamental principles governing catalytic activity. By integrating computational methods with experimental validation, researchers can systematically explore the vast design space of M-N-C catalysts, leading to the development of highly efficient and durable materials. This synergy between computation and experimentation is essential for the rational design of next-generation ORR catalysts, paving the way for their practical application in energy conversion and storage technologies.

DECLARATIONS

Authors' contributions

Proposed the topic of this review: Kou, Z.
Wrote the manuscript: Zhang, D.; Zhang, X.
Designed and drew the figures: Zhang, D.; Li, X.; Zhang, X.
Collectively discussed and revised the manuscript: Zhang, D.; Li, X.; Zhang, X.; Feng, C.; Kou, Z.; Chu, Y.; Chen, C.

Availability of data and materials

Not applicable.

Financial support and sponsorship

The work is financially supported by the Natural Science Foundation of Hubei Province (Grant No.2022CFB388), Natural Science Foundation of Hainan Province of China (Grant No.623MS068), National College Student Innovation and Entrepreneurship Training Program (S202310497121).

Conflicts of interest

All authors declared that there are no conflicts of interest.

Ethical approval and consent to participate

Not applicable.

Consent for publication

Not applicable.

REFERENCES

1. Wang, X. X.; Swihart, M. T.; Wu, G. Achievements, challenges and perspectives on cathode catalysts in proton exchange membrane fuel cells for transportation. *Nat. Catal.* **2019**, *2*, 578-89. DOI
2. Xia, Q.; Zhai, Y.; Zhao, L.; et al. Carbon-supported single-atom catalysts for advanced rechargeable metal-air batteries. *Energy. Mater.* **2022**, *2*, 200015. DOI

3. Staffell, I.; Scamman, D.; Velazquez, A. A.; et al. The role of hydrogen and fuel cells in the global energy system. *Energy. Environ. Sci.* **2019**, *12*, 463-91. DOI
4. Yeager, E. Electrocatalysts for O_2 reduction. *Electrochim. Acta.* **1984**, *29*, 1527-37. DOI
5. Gong, X.; Song, P.; Han, C.; Xiao, Y.; Mei, X.; Xu, W. Heterogeneous single-atom catalysts for energy process: recent progress, applications and challenges. *Energy. Mater.* **2023**, *3*, 300016. DOI
6. Li, Z.; Yang, C.; Xu, B.; Yao, L.; Zhu, W.; Cui, Y. Electrochemically nitrate remediation by single-atom catalysts: advances, mechanisms, and prospects. *Energy. Mater.* **2024**, *4*, 400046. DOI
7. Zitolo, A.; Goellner, V.; Armel, V.; et al. Identification of catalytic sites for oxygen reduction in iron- and nitrogen-doped graphene materials. *Nat. Mater.* **2015**, *14*, 937-42. DOI
8. Jia, Q.; Ramaswamy, N.; Hafiz, H.; et al. Experimental observation of redox-induced Fe-N switching behavior as a determinant role for oxygen reduction activity. *ACS. Nano.* **2015**, *9*, 12496-505. DOI
9. Wu, F.; Pan, C.; He, C. T.; et al. Single-atom Co-N_4 electrocatalyst enabling four-electron oxygen reduction with enhanced hydrogen peroxide tolerance for selective sensing. *J. Am. Chem. Soc.* **2020**, *142*, 16861-7. DOI
10. Li, Z.; Ji, S.; Xu, C.; et al. Engineering the electronic structure of single-atom iron sites with boosted oxygen bifunctional activity for zinc-air batteries. *Adv. Mater.* **2023**, *35*, e2209644. DOI
11. He, Y.; Wu, G. PGM-free oxygen-reduction catalyst development for proton-exchange membrane fuel cells: challenges, solutions, and promises. *ACC. Mater. Res.* **2022**, *3*, 224-36. DOI
12. Ji, S.; Jiang, B.; Hao, H.; et al. Matching the kinetics of natural enzymes with a single-atom iron nanozyme. *Nat. Catal.* **2021**, *4*, 407-17. DOI
13. Li, X.; Yang, X.; Liu, L.; et al. Chemical vapor deposition for N/S-doped single Fe site catalysts for the oxygen reduction in direct methanol fuel cells. *ACS. Catal.* **2021**, *11*, 7450-9. DOI
14. Zhou, S.; Chen, C.; Xia, J.; et al. FeN_3S_1-OH single-atom sites anchored on hollow porous carbon for highly efficient pH-universal oxygen reduction reaction. *Small* **2024**, *20*, e2310224. DOI
15. Peng, L.; Yang, J.; Yang, Y.; et al. Mesopore-rich Fe-N-C catalyst with FeN_4-O-NC single-atom sites delivers remarkable oxygen reduction reaction performance in alkaline media. *Adv. Mater.* **2022**, *34*, e2202544. DOI
16. Zhao, K.; Liu, S.; Li, Y.; et al. Insight into the mechanism of axial ligands regulating the catalytic activity of Fe-N_4 sites for oxygen reduction reaction. *Adv. Energy. Mater.* **2022**, *12*, 2103588. DOI
17. Sarma, B. B.; Maurer, F.; Doronkin, D. E.; Grunwaldt, J. D. Design of single-atom catalysts and tracking their fate using *operando* and advanced X-ray spectroscopic tools. *Chem. Rev.* **2023**, *123*, 379-444. DOI PubMed PMC
18. Chen, Y.; Ji, S.; Zhao, S.; et al. Enhanced oxygen reduction with single-atomic-site iron catalysts for a zinc-air battery and hydrogen-air fuel cell. *Nat. Commun.* **2018**, *9*, 5422. DOI PubMed PMC
19. Yin, H.; Yuan, P.; Lu, B.; et al. Phosphorus-driven electron delocalization on edge-type FeN_4 active sites for oxygen reduction in acid medium. *ACS. Catal.* **2021**, *11*, 12754-62. DOI
20. Wang, L.; Tian, W. W.; Zhang, W.; Yu, F.; Yuan, Z. Y. Boosting oxygen electrocatalytic performance of Cu atom by engineering the d-band center via secondary heteroatomic phosphorus modulation. *Appl. Catal. B. Environ.* **2023**, *338*, 123043. DOI
21. Qin, J.; Liu, H.; Zou, P.; Zhang, R.; Wang, C.; Xin, H. L. Altering ligand fields in single-atom sites through second-shell anion modulation boosts the oxygen reduction reaction. *J. Am. Chem. Soc.* **2022**, *144*, 2197-207. DOI
22. Liu, J.; Chen, W.; Yuan, S.; Liu, T.; Wang, Q. High-coordination Fe-N_4SP single-atom catalysts *via* the multi-shell synergistic effect for the enhanced oxygen reduction reaction of rechargeable Zn-air battery cathodes. *Energy. Environ. Sci.* **2024**, *17*, 249-59. DOI
23. Chen, Z.; Niu, H.; Ding, J.; et al. Unraveling the origin of sulfur-doped Fe-N-C single-atom catalyst for enhanced oxygen reduction activity: effect of iron spin-state tuning. *Angew. Chem. Int. Ed.* **2021**, *60*, 25404-10. DOI
24. Zhao, Y.; Shen, Z.; Huo, J.; et al. Epoxy-rich Fe single atom sites boost oxygen reduction electrocatalysis. *Angew. Chem. Int. Ed.* **2023**, *62*, e202308349. DOI
25. Shen, G.; Zhang, R.; Pan, L.; et al. Regulating the spin state of Fe^{III} by atomically anchoring on ultrathin titanium dioxide for efficient oxygen evolution electrocatalysis. *Angew. Chem. Int. Ed.* **2020**, *59*, 2313-7. DOI
26. Zhang, J.; Zhao, Y.; Chen, C.; et al. Tuning the coordination environment in single-atom catalysts to achieve highly efficient oxygen reduction reactions. *J. Am. Chem. Soc.* **2019**, *141*, 20118-26. DOI
27. Zhou, Y.; Lu, R.; Tao, X.; et al. Boosting oxygen electrocatalytic activity of Fe-N-C catalysts by phosphorus incorporation. *J. Am. Chem. Soc.* **2023**, *145*, 3647-55. DOI PubMed PMC
28. Chang, H.; Guo, Y. F.; Liu, X.; Wang, P. F.; Xie, Y.; Yi, T. F. Dual MOF-derived Fe/N/P-tridoped carbon nanotube as high-performance oxygen reduction catalysts for zinc-air batteries. *Appl. Catal. B. Environ.* **2023**, *327*, 122469. DOI
29. Huang, Z. F.; Song, J.; Dou, S.; Li, X.; Wang, J.; Wang, X. Strategies to break the scaling relation toward enhanced oxygen electrocatalysis. *Matter* **2019**, *1*, 1494-518. DOI
30. Han, J.; Tan, H.; Guo, K.; et al. The "pull effect" of a hanging ZnII on improving the four-electron oxygen reduction selectivity with Co porphyrin. *Angew. Chem. Int. Ed.* **2024**, *63*, e202409793. DOI
31. Wang, Z.; Cheng, M.; Liu, Y.; et al. Dual-atomic-site catalysts for molecular oxygen activation in heterogeneous thermo-/electro-catalysis. *Angew. Chem. Int. Ed.* **2023**, *62*, e202301483. DOI
32. Wei, S.; Yang, R.; Wang, Z.; Zhang, J.; Bu, X. H. Planar chlorination engineering: a strategy of completely breaking the geometric symmetry of Fe-N_4 site for boosting oxygen electroreduction. *Adv. Mater.* **2024**, *36*, e2404692. DOI

33. Yin, L.; Zhang, S.; Sun, M.; Wang, S.; Huang, B.; Du, Y. Heteroatom-driven coordination fields altering single cerium atom sites for efficient oxygen reduction reaction. *Adv. Mater.* **2023**, *35*, 2302485. DOI
34. Li, H.; Zhao, H.; Yan, G.; et al. Ternary heteroatomic doping induced microenvironment engineering of low Fe-N_4-loaded carbon nanofibers for bifunctional oxygen electrocatalysis. *Small* **2024**, *20*, e2304844. DOI
35. Sun, Z.; Zhang, H.; Cao, L.; et al. Understanding synergistic catalysis on Cu-Se dual atom sites via *operando* X-ray absorption spectroscopy in oxygen reduction reaction. *Angew. Chem. Int. Ed.* **2023**, *62*, e202217719. DOI
36. Niu, Z.; Lu, Z.; Qiao, Z.; et al. Long-range regulation of Se doping for oxygen reduction of atomically dispersed Sb catalysts for ultralow-temperature solid-state Zn-air batteries. *ACS. Catal.* **2023**, *13*, 7122-31. DOI
37. Wang, Q.; Kaushik, S.; Xiao, X.; Xu, Q. Sustainable zinc-air battery chemistry: advances, challenges and prospects. *Chem. Soc. Rev.* **2023**, *52*, 6139-90. DOI
38. Liu, S.; Wang, Z.; Zhou, S.; et al. Metal-organic-framework-derived hybrid carbon nanocages as a bifunctional electrocatalyst for oxygen reduction and evolution. *Adv. Mater.* **2017**, *29*, 1700874. DOI
39. Liu, M.; Li, N.; Cao, S.; et al. A "pre-constrained metal twins" strategy to prepare efficient dual-metal-atom catalysts for cooperative oxygen electrocatalysis. *Adv. Mater.* **2022**, *34*, 2107421. DOI
40. Chen, J.; Li, H.; Fan, C.; et al. Dual single-atomic Ni-N_4 and Fe-N_4 sites constructing janus hollow graphene for selective oxygen electrocatalysis. *Adv. Mater.* **2020**, *32*, 2003134. DOI
41. Guo, D.; Shibuya, R.; Akiba, C.; Saji, S.; Kondo, T.; Nakamura, J. Active sites of nitrogen-doped carbon materials for oxygen reduction reaction clarified using model catalysts. *Science* **2016**, *351*, 361-5. DOI PubMed
42. Yu, W.; Huang, H.; Qin, Y.; et al. The synergistic effect of pyrrolic-N and pyridinic-N with Pt under strong metal-support interaction to achieve high-performance alkaline hydrogen evolution. *Adv. Energy. Mater.* **2022**, *12*, 2200110. DOI
43. Zitolo, A.; Ranjbar-Sahraie, N.; Mineva, T.; et al. Identification of catalytic sites in cobalt-nitrogen-carbon materials for the oxygen reduction reaction. *Nat. Commun.* **2017**, *8*, 957. DOI PubMed PMC
44. Zhang, N.; Zhou, T.; Chen, M.; et al. High-purity pyrrole-type FeN_4 sites as a superior oxygen reduction electrocatalyst. *Energy. Environ. Sci.* **2020**, *13*, 111-8. DOI
45. Yang, H.; Gao, S.; Rao, D.; Yan, X. Designing superior bifunctional electrocatalyst with high-purity pyrrole-type CoN_4 and adjacent metallic cobalt sites for rechargeable Zn-air batteries. *Energy. Storage. Mater.* **2022**, *46*, 553-62. DOI
46. Ha, Y.; Fei, B.; Yan, X.; et al. Atomically dispersed Co-pyridinic N-C for superior oxygen reduction reaction. *Adv. Energy. Mater.* **2020**, *10*, 2002592. DOI
47. Li, L.; Wen, Y.; Han, G.; et al. Tailoring the stability of Fe-N-C via pyridinic nitrogen for acid oxygen reduction reaction. *Chem. Eng. J.* **2022**, *437*, 135320. DOI
48. Ni, L.; Gallenkamp, C.; Wagner, S.; Bill, E.; Krewald, V.; Kramm, U. I. Identification of the catalytically dominant iron environment in iron- and nitrogen-doped carbon catalysts for the oxygen reduction reaction. *J. Am. Chem. Soc.* **2022**, *144*, 16827-40. DOI PubMed
49. Hu, X.; Chen, S.; Chen, L.; et al. What is the real origin of the activity of Fe-N-C electrocatalysts in the O_2 reduction reaction? Critical roles of coordinating pyrrolic N and axially adsorbing species. *J. Am. Chem. Soc.* **2022**, *144*, 18144-52. DOI
50. Gu, Y.; Nie, N.; Liu, J.; et al. Enriching H_2O through boron nitride as a support to promote hydrogen evolution from non-filtered seawater. *EcoEnergy* **2023**, *1*, 405-13. DOI
51. Liu, S.; Shi, Q.; Wu, G. Solving the activity-stability trade-off riddle. *Nat. Catal.* **2021**, *4*, 6-7. DOI
52. Cui, L.; Zhao, X.; Xie, H.; Zhang, Z. Overcoming the activity-stability trade-off in heterogeneous electro-Fenton catalysis: encapsulating carbon cloth-supported iron oxychloride within graphitic layers. *ACS. Catal.* **2022**, *12*, 13334-48. DOI
53. Li, J.; Sougrati, M. T.; Zitolo, A.; et al. Identification of durable and non-durable FeN_x sites in Fe-N-C materials for proton exchange membrane fuel cells. *Nat. Catal.* **2021**, *4*, 10-9. DOI
54. Liu, S.; Li, C.; Zachman, M. J.; et al. Atomically dispersed iron sites with a nitrogen-carbon coating as highly active and durable oxygen reduction catalysts for fuel cells. *Nat. Energy.* **2022**, *7*, 652-63. DOI
55. Bai, J.; Zhao, T.; Xu, M.; et al. Monosymmetric Fe-N_4 sites enabling durable proton exchange membrane fuel cell cathode by chemical vapor modification. *Nat. Commun.* **2024**, *15*, 4219. DOI PubMed PMC
56. Wang, W.; Jia, Q.; Mukerjee, S.; Chen, S. Recent insights into the oxygen-reduction electrocatalysis of Fe/N/C materials. *ACS. Catal.* **2019**, *9*, 10126-41. DOI
57. Zhang, H.; Hwang, S.; Wang, M.; et al. Single atomic iron catalysts for oxygen reduction in acidic media: particle size control and thermal activation. *J. Am. Chem. Soc.* **2017**, *139*, 14143-9. DOI
58. Ni, B.; Shen, P.; Zhang, G.; et al. Second-shell N dopants regulate acidic O_2 reduction pathways on isolated Pt sites. *J. Am. Chem. Soc.* **2024**, *146*, 11181-92. DOI
59. Liu, L.; Corma, A. Metal catalysts for heterogeneous catalysis: from single atoms to nanoclusters and nanoparticles. *Chem. Rev.* **2018**, *118*, 4981-5079. DOI PubMed PMC
60. Lu, J.; Lu, Q.; Guo, Y.; et al. Cobalt atom-cluster interactions synergistically enhance the activity of oxygen reduction reaction in seawater. *Energy. Storage. Mater.* **2024**, *65*, 103093. DOI
61. Wang, Z.; Lu, Z.; Ye, Q.; et al. Construction of Fe nanoclusters/nanoparticles to engineer FeN_4 sites on multichannel porous carbon fibers for boosting oxygen reduction reaction. *Adv. Funct. Mater.* **2024**, *34*, 2315150. DOI
62. Liang, C.; Han, X.; Zhang, T.; et al. Cu nanoclusters accelerate the rate-determining step of oxygen reduction on Fe-N-C in all pH

range. *Adv. Energy. Mater.* **2024**, *14*, 2303935. DOI

63. Chen, Y.; Kong, X.; Wang, Y.; et al. A binary single atom Fe_3C|Fe-N-C catalyst by an atomic fence evaporation strategy for high performance ORR/OER and flexible zinc-air battery. *Chem. Eng. J.* **2023**, *454*, 140512. DOI
64. Chang, J.; Zhang, Q.; Yu, J.; et al. A Fe single atom seed-mediated strategy toward Fe_3C/Fe-N-C catalysts with outstanding bifunctional ORR/OER activities. *Adv. Sci.* **2023**, *10*, e2301656. DOI PubMed PMC
65. Zhu, W.; Pei, Y.; Douglin, J. C.; et al. Multi-scale study on bifunctional Co/Fe-N-C cathode catalyst layers with high active site density for the oxygen reduction reaction. *Appl. Catal. B. Environ.* **2021**, *299*, 120656. DOI
66. Wu, Y.; Chen, L.; Geng, S.; et al. PtFe nanoalloys supported on Fe-based cubic framework as efficient oxygen reduction electrocatalysts for proton exchange membrane fuel cells. *Adv. Funct. Mater.* **2024**, *34*, 2307297. DOI
67. Wang, F.; Yang, J.; Li, J.; et al. Which is best for ORR: single atoms, nanoclusters, or coexistence? *ACS. Energy. Lett.* **2024**, *9*, 93-101. DOI
68. Liu, M.; Lee, J.; Yang, T. C.; et al. Synergies of Fe single atoms and clusters on N-doped carbon electrocatalyst for pH-universal oxygen reduction. *Small. Methods.* **2021**, *5*, e2001165. DOI
69. Han, A.; Sun, W.; Wan, X.; et al. Construction of Co_4 atomic clusters to enable Fe-N_4 motifs with highly active and durable oxygen reduction performance. *Angew. Chem. Int. Ed.* **2023**, *62*, e202303185. DOI
70. Li, Y.; Li, Z.; Shi, K.; et al. Single-atom Mn catalysts via integration with Mn sub nano-clusters synergistically enhance oxygen reduction reaction. *Small* **2024**, *20*, e2309727. DOI
71. Yuan, L. J.; Liu, B.; Shen, L. X.; et al. d-orbital electron delocalization realized by axial Fe_4C atomic clusters delivers high-performance Fe-N-C catalysts for oxygen reduction reaction. *Adv. Mater.* **2023**, *35*, e2305945. DOI
72. Jiang, W. J.; Gu, L.; Li, L.; et al. Understanding the high activity of Fe-N-C electrocatalysts in oxygen reduction: Fe/Fe_3C nanoparticles boost the activity of Fe-N_x. *J. Am. Chem. Soc.* **2016**, *138*, 3570-8. DOI
73. Chen, G.; Liu, Y.; Xue, S.; et al. Exceptionally bifunctional ORR/OER performance via synergistic atom-cluster interaction. *Small* **2024**, *20*, e2308192. DOI
74. Cui, X.; Gao, L.; Lei, S.; et al. Simultaneously crafting single-atomic Fe sites and graphitic layer-wrapped Fe_3C nanoparticles encapsulated within mesoporous carbon tubes for oxygen reduction. *Adv. Funct. Mater.* **2021**, *31*, 2009197. DOI
75. Wei, X.; Song, S.; Wu, N.; et al. Synergistically enhanced single-atomic site Fe by Fe_3C@C for boosted oxygen reduction in neutral electrolyte. *Nano. Energy.* **2021**, *84*, 105840. DOI
76. Lee, Y.; Ahn, J. H.; Jang, H.; et al. Very strong interaction between FeN_4 and titanium carbide for durable 4-electron oxygen reduction reaction suppressing catalyst deactivation by peroxide. *J. Mater. Chem. A.* **2022**, *10*, 24041-50. DOI
77. Pan, Y.; Li, M.; Mi, W.; et al. Single-atomic Mn sites coupled with Fe_3C nanoparticles encapsulated in carbon matrixes derived from bimetallic Mn/Fe polyphthalocyanine conjugated polymer networks for accelerating electrocatalytic oxygen reduction. *Nano. Res.* **2022**, *15*, 7976-85. DOI
78. Xu, C.; Guo, C.; Liu, J.; et al. Accelerating the oxygen adsorption kinetics to regulate the oxygen reduction catalysis via Fe_3C nanoparticles coupled with single Fe-N_4 sites. *Energy. Storage. Mater.* **2022**, *51*, 149-58. DOI
79. Bae, G.; Han, S.; Oh, H. S.; Choi, C. H. Operando stability of single-atom electrocatalysts. *Angew. Chem. Int. Ed.* **2023**, *62*, e202219227. DOI
80. Choi, C. H.; Lim, H. K.; Chung, M. W.; et al. The Achilles' heel of iron-based catalysts during oxygen reduction in an acidic medium. *Energy. Environ. Sci.* **2018**, *11*, 3176-82. DOI
81. Bae, G.; Chung, M. W.; Ji, S. G.; Jaouen, F.; Choi, C. H. pH effect on the H_2O_2-induced deactivation of Fe-N-C catalysts. *ACS. Catal.* **2020**, *10*, 8485-95. DOI
82. Li, Y.; Chen, M. Y.; Lu, B. A.; Wu, H. R.; Zhang, J. N. Unravelling the role of hydrogen peroxide in pH-dependent ORR performance of Mn-N-C catalysts. *Appl. Catal. B. Environ.* **2024**, *342*, 123458. DOI
83. Luo, E.; Zhang, H.; Wang, X.; et al. Single-atom Cr-N_4 sites designed for durable oxygen reduction catalysis in acid media. *Angew. Chem. Int. Ed.* **2019**, *58*, 12469-75. DOI
84. Guo, Y.; Wang, C.; Xiao, Y.; et al. Stabilizing Fe single atom catalysts by implanting Cr atomic clusters to boost oxygen reduction reaction. *Appl. Catal. B. Environ. Energy.* **2024**, *344*, 123679. DOI
85. Lawler, R.; Cho, J.; Ham, H. C.; et al. CeO_2 (111) surface with oxygen vacancy for radical scavenging: a density functional theory approach. *J. Phys. Chem. C.* **2020**, *124*, 20950-9. DOI
86. Karakoti, A.; Singh, S.; Dowding, J. M.; Seal, S.; Self, W. T. Redox-active radical scavenging nanomaterials. *Chem. Soc. Rev.* **2010**, *39*, 4422-32. DOI
87. Xie, H.; Xie, X.; Hu, G.; et al. Ta-TiO_x nanoparticles as radical scavengers to improve the durability of Fe-N-C oxygen reduction catalysts. *Nat. Energy.* **2022**, *7*, 281-9. DOI
88. Li, J.; Maurya, S.; Kim, Y. S.; et al. Stabilizing single-atom iron electrocatalysts for oxygen reduction via ceria confining and trapping. *ACS. Catal.* **2020**, *10*, 2452-8. DOI
89. Cheng, X.; Jiang, X.; Yin, S.; et al. Instantaneous free radical scavenging by CeO_2 nanoparticles adjacent to the Fe-N_4 active sites for durable fuel cells. *Angew. Chem. Int. Ed.* **2023**, *62*, e202306166. DOI
90. Gao, X. B.; Wang, Y.; Xu, W.; et al. Mechanism of particle-mediated inhibition of demetalation for single-atom catalytic sites in acidic electrochemical environments. *J. Am. Chem. Soc.* **2023**, *145*, 15528-37. DOI
91. Bae, G.; Kim, M. M.; Han, M. H.; et al. Unravelling the complex causality behind Fe-N-C degradation in fuel cells. *Nat. Catal.* **2023**,

6, 1140-50. DOI
92. Mechler, A. K.; Sahraie, N. R.; Armel, V.; et al. Stabilization of iron-based fuel cell catalysts by non-catalytic platinum. *J. Electrochem. Soc.* **2018**, *165*, F1084-91. DOI
93. Xiao, F.; Wang, Q.; Xu, G. L.; et al. Atomically dispersed Pt and Fe sites and Pt-Fe nanoparticles for durable proton exchange membrane fuel cells. *Nat. Catal.* **2022**, *5*, 503-12. DOI
94. Zhou, H.; Yang, T.; Kou, Z.; et al. Negative pressure pyrolysis induced highly accessible single sites dispersed on 3D graphene frameworks for enhanced oxygen reduction. *Angew. Chem. Int. Ed.* **2020**, *59*, 20465-9. DOI
95. Yu, Y.; Lv, Z.; Liu, Z.; et al. Activation of Ga liquid catalyst with continuously exposed active sites for electrocatalytic C-N coupling. *Angew. Chem. Int. Ed.* **2024**, *63*, e202402236. DOI
96. Yuan, S.; Peng, J.; Zhang, Y.; et al. Tuning the catalytic activity of Fe-phthalocyanine-based catalysts for the oxygen reduction reaction by ligand functionalization. *ACS. Catal.* **2022**, *12*, 7278-87. DOI
97. Fei, H.; Dong, J.; Chen, D.; et al. Single atom electrocatalysts supported on graphene or graphene-like carbons. *Chem. Soc. Rev.* **2019**, *48*, 5207-41. DOI PubMed
98. Zhao, Z.; Xiong, Y.; Yu, S.; et al. Single-atom Zn with nitrogen defects on biomimetic 3D carbon nanotubes for bifunctional oxygen electrocatalysis. *J. Colloid. Interface. Sci.* **2023**, *650*, 934-42. DOI
99. Li, L.; Liu, X.; Wang, J.; et al. Atomically dispersed Co in a cross-channel hierarchical carbon-based electrocatalyst for high-performance oxygen reduction in Zn-air batteries. *J. Mater. Chem. A.* **2022**, *10*, 18723-9. DOI
100. Tian, H.; Song, A.; Zhang, P.; et al. High durability of Fe-N-C single atom catalysts with carbon vacancies towards oxygen reduction reaction in alkaline media. *Adv. Mater.* **2023**, *35*, 2210714. DOI
101. Liu, K.; Fu, J.; Lin, Y.; et al. Insights into the activity of single-atom Fe-N-C catalysts for oxygen reduction reaction. *Nat. Commun.* **2022**, *13*, 2075. DOI PubMed PMC
102. Wang, X.; Jia, Y.; Mao, X.; et al. Edge-rich Fe-N_4 active sites in defective carbon for oxygen reduction catalysis. *Adv. Mater.* **2020**, *32*, e2000966. DOI
103. Fu, X.; Li, N.; Ren, B.; et al. Tailoring FeN_4 sites with edge enrichment for boosted oxygen reduction performance in proton exchange membrane fuel cell. *Adv. Energy. Mater.* **2019**, *9*, 1803737. DOI
104. Kong, F.; Huang, Y.; Chen, M.; et al. Creation of densely exposed and cavity-edged single Fe active sites for enhanced oxygen electroreduction. *Appl. Catal. B. Environ.* **2022**, *317*, 121768. DOI
105. Zhang, R.; Xue, B.; Tao, Y.; et al. Edge-site engineering of defective Fe-N_4 nanozymes with boosted catalase-like performance for retinal vasculopathies. *Adv. Mater.* **2022**, *34*, e2205324. DOI
106. Cui, L.; Zhao, J.; Liu, G.; Wang, Z.; Li, B.; Zong, L. Rich edge-hosted single-atomic Cu-N_4 sites for highly efficient oxygen reduction reaction performance. *J. Colloid. Interface. Sci.* **2022**, *622*, 209-17. DOI
107. Mun, Y.; Lee, S.; Kim, K.; et al. Versatile strategy for tuning ORR activity of a single Fe-N_4 site by controlling electron-withdrawing/donating properties of a carbon plane. *J. Am. Chem. Soc.* **2019**, *141*, 6254-62. DOI
108. Gu, Y.; Xi, B. J.; Zhang, H.; Ma, Y. C.; Xiong, S. L. Activation of main-group antimony atomic sites for oxygen reduction catalysis. *Angew. Chem. Int. Ed.* **2022**, *61*, e202202200. DOI
109. Chang, X.; Xu, S.; Wang, D.; Zhang, Z.; Guo, Y.; Kang, S. Flash dual-engineering of surface carboxyl defects and single Cu atoms of g-C_3N_4 via unique CO_2 plasma immersion approach for boosted photocatalytic activity. *Mater. Today. Adv.* **2022**, *15*, 100274. DOI
110. Lv, M.; Cui, C. X.; Huang, N.; et al. Precisely engineering asymmetric atomic CoN_4 by electron donating and extracting for oxygen reduction reaction. *Angew. Chem. Int. Ed.* **2024**, *63*, e202315802. DOI
111. Wei, X.; Jiang, C.; Xu, H.; et al. Synergistic effect of organic ligands on metal site spin states in 2D metal-organic frameworks for enhanced ORR performance. *ACS. Catal.* **2023**, *13*, 15663-72. DOI
112. Liu, M.; Sun, T.; Peng, T.; et al. Fe-NC single-atom catalyst with hierarchical porous structure and P-O bond coordination for oxygen reduction. *ACS. Energy. Lett.* **2023**, *8*, 4531-9. DOI
113. Tang, C.; Chen, L.; Li, H.; et al. Tailoring acidic oxygen reduction selectivity on single-atom catalysts via modification of first and second coordination spheres. *J. Am. Chem. Soc.* **2021**, *143*, 7819-27. DOI
114. Qiao, Y.; Yuan, P.; Hu, Y.; et al. Sulfuration of an Fe-N-C catalyst containing Fe_xC/Fe species to enhance the catalysis of oxygen reduction in acidic media and for use in flexible Zn-air batteries. *Adv. Mater.* **2018**, *30*, e1804504. DOI
115. Chi, B.; Zhang, L.; Yang, X.; et al. Promoting ZIF-8-derived Fe-N-C oxygen reduction catalysts via Zr doping in proton exchange membrane fuel cells: durability and activity enhancements. *ACS. Catal.* **2023**, *13*, 4221-30. DOI
116. Zhu, P.; Xiong, X.; Wang, X.; et al. Regulating the FeN_4 moiety by constructing Fe-Mo dual-metal atom sites for efficient electrochemical oxygen reduction. *Nano. Lett.* **2022**, *22*, 9507-15. DOI
117. Zhang, M.; Li, H.; Chen, J.; et al. High-loading Co single atoms and clusters active sites toward enhanced electrocatalysis of oxygen reduction reaction for high-performance Zn-air battery. *Adv. Funct. Mater.* **2023**, *33*, 2209726. DOI
118. Liu, H.; Jiang, L.; Khan, J.; et al. Decorating single-atomic Mn sites with FeMn clusters to boost oxygen reduction reaction. *Angew. Chem. Int. Ed.* **2023**, *62*, e202214988. DOI
119. Wei, X.; Song, S.; Cai, W.; et al. Pt nanoparticle-Mn single-atom pairs for enhanced oxygen reduction. *ACS. Nano.* **2024**, *18*, 4308-19. DOI
120. Xu, X.; Li, X.; Lu, W.; et al. Collective effect in a multicomponent ensemble combining single atoms and nanoparticles for efficient and durable oxygen reduction. *Angew. Chem. Int. Ed. Engl.* **2024**, *63*, e202400765. DOI

121. Zhang, Y.; Chen, Z. W.; Liu, X.; et al. Vacancy-enhanced Sb-N_4 sites for the oxygen reduction reaction and Zn-air battery. *Nano. Lett.* **2024**, *24*, 4291-9. DOI
122. Lyu, L.; Hu, X.; Lee, S.; et al. Oxygen reduction kinetics of Fe-N-C single atom catalysts boosted by pyridinic N vacancy for temperature-adaptive Zn-air batteries. *J. Am. Chem. Soc.* **2024**, *146*, 4803-13. DOI
123. Liu, H.; Jiang, L.; Sun, Y.; et al. Revisiting the role of sulfur functionality in regulating the electron distribution of single-atomic Fe sites toward enhanced oxygen reduction. *Adv. Funct. Mater.* **2023**, *33*, 2304074. DOI
124. Qu, Y.; Li, Z.; Chen, W.; et al. Direct transformation of bulk copper into copper single sites via emitting and trapping of atoms. *Nat. Catal.* **2018**, *1*, 781-6. DOI
125. Liu, H.; Li, J.; Arbiol, J.; Yang, B.; Tang, P. Catalytic reactivity descriptors of metal-nitrogen-doped carbon catalysts for electrocatalysis. *EcoEnergy* **2023**, *1*, 154-85. DOI